Technology Development for Iron and Cobalt Fischer-Tropsch Catalysts

Quarterly Report

July 1, 1999 to September 30, 1999

Burtron H. Davis

Enrique Iglesia (UC/B Subcontract)

November, 1999

DE-FC26-98FT40308

University of Kentucky Research Foundation

201 Kinkead Hall

Lexington, KY 40506

University of California-Berkelely (Subcontract)

Laboratory for the Science and Application of Catalysis

Department of Chemical Engineering

University of California at Berkeley

Berkeley, CA 94720

Abstract

CAER

The impact of deuterium on the Fischer-Tropsch (FT) synthesis was studied with a precipitated iron catalyst in the slurry phase. Deuterium has been used by several research groups to better understand the mechanism of CO hydrogenation. Inverse ($k_H/k_D < 1$), normal ($k_H/k_D > 1$) and no isotope effect ($k_H/k_D = 1$) have been reported. The conflicting results are thought to arise because rate of reaction is a combination of kinetic and equilibrium factors.

In summary, the presence of boron produced only minor changes on the properties of the cobalt catalyst. In earlier studies, it was shown that the presence of boron made the catalyst less susceptible to poisoning by sulfur.

Steady-state supercritical Fischer-Tropsch synthesis was studied in our work using a fixed-bed reactor and an unpromoted Co/SiO_2 catalyst. This serves as the baseline for promoted catalyst studies. A pentane-hexane mixture was used as the supercitical solvent. Overall reactor pressure, syngas partial pressure and contact time were kept constant to obtain a valid comparison of the impact of solvent density in the catalytic activity and selectivity. Three different partial pressures of the mixture were chosen based on the density-pressure curve in order to investigate the pressure tuning effect to Fischer-Tropsch synthesis near critical region.

UC/B

In-situ Fe K-edge X-ray absorption spectroscopic (XAS) measurement of Fe_2O_3 in synthesis gas at 250°C showed that Fe_2O_3 was converted to a mixture of Fe_3O_4 and Fe carbides after 9 h. The linear combination of the X-ray absorption near edge spectroscopy (LC XANES) fit of the samples provided by the Center for Applied Energy Research (CAER) of the University of Kentucky showed that the samples used for various lengths of time for FTS contained both Fe carbides and Fe_3O_4, and the extent of carburization increased and reached a highest value and then decreased gradually with time on stream. After 432 h, all the Fe carbides were converted to Fe_3O_4. The isotopic effects using synthesis gases of $D_2/CO/N_2$ and $H_2/CO/N_2$ on an Fe-Zn catalyst (Zn/Fe=0.1, K/M=0.02, Cu/Fe=0.01) at 235°C and 21.4 atm showed that lower methane and CO_2 selectivities and a higher selectivity to C_{5+} were obtained with $H_2/CO/N_2$ than with $D_2/CO/N_2$. Inverse isotopic effects for CO conversion rate and hydrocarbon formation rate and a normal isotopic effect for CO_2 formation were observed when D_2 was used instead of H_2. The k_H/k_D ratio for hydrocarbon formation decreased with increasing CO conversion and with increasing carbon number. The isotopic effects were more evident for the formation of hydrocarbons with higher molecular weight, and for the formation of paraffins than for olefins. Kinetic studies and the H_2/D_2 isotope effects during FTS with both CO/H_2 and CO/D_2 were carried out over a 21.9 wt.% Co/SiO_2 catalyst at 200°C and 20 atm. The CO consumption rate data along with those obtained from the previous kinetic run were fitted to rate expressions on the basis of our proposed mechanisms with multivariable non-linear regression. The kinetic isotope effects for CO consumption and for individual hydrocarbons C_1-C_7 were obtained by comparing the corresponding reaction rates with H_2 and D_2. Inverse kinetic isotope effects were obtained for CO consumption ($k_H/k_D = 0.8$) when the CO conversions were between 10% and 40%. The results showed that the isotope effects (k_H/k_D) were generally inverse for paraffins whereas normal for olefins at low conversions when the effect of secondary reactions could be neglected. These isotope effects resulted from a combination of kinetic and equilibrium isotopic effects which may be associated with individual elementary steps.

Table of Contents

Executive Summary

CAER

Steady-state supercritical Fischer-Tropsch synthesis was studied using a fixed-bed reactor and a Co/SiO_2 catalyst. A pentane-hexane mixture was used as the supercitical solvent. Overall reactor pressure, syngas partial pressure and contact time were kept constant to obtain valid comparisons.

Three different partial pressure points of the mixture were chosen based on the density-pressure curve to investigate the pressure tuning effect for Fischer-Tropsch synthesis near critical region. It was found that supercitical phase Fischer-Tropsch synthesis can significantly inhibit the deactivation of catalyst due to the extraction of heavy hydrocarbon products from catalyst pores and possibly improving the heat transfer in plug-flow reactor. The highest CO conversion was obtained when the solvent partial pressure is just above its critical pressure compared to its more gas-like or liquid- like state. Reproducible data were obtained by repeating the conditions.

Methane and carbon dioxide selectivity decreased dramatically with an increase of pentane-hexane partial pressure. The selectivity of reaction and α value of different conditions will be defined in future work.

The vapor-liquid equilibrium has the potential to dramatically impact the results for slurry bubble column operations (e.g., last quarterly report). Data are not available to allow one to assess the impact of vapor-equilibrium on the slurry reactor operation. To obtain data to evaluate this effect, we have synthesized deuterated FT products to add during synthesis with H_2/CO in order to obtain retention times in the reactor for various carbon number products and thereby obtain experimental values for vapor-liquid under reaction conditions. These results will greatly aid in reactor design and in the evaluation of various separation procedures. In addition, these

studies allow us to compare isotopic data from the CAER CSTR with those obtained at Berkeley in fixed bed reactors. These studies also serve to integrate the research activities of the two labs.

The isotope effect with deuterium is probably the combination of equilibrium and kinetic effects. The proposed steps for the hydrogenation of carbon monoxide are:

$$H_2 \overset{K_{H'}}{\leftrightarrows} (H_2)_s \overset{K_{H''}}{\leftrightarrows} 2H_s \tag{1}$$

$$CO \overset{K_{CO'}}{\leftrightarrows} CO_s \overset{K_{CO''}}{\leftrightarrows} C_s + Os \tag{2}$$

$$C_s + H_s \overset{k_1}{\leftrightarrows} CH_s \overset{k_2}{\leftrightarrows} CH_{2,s} \overset{k_3}{\leftrightarrows} CH_{3,s} \overset{k_4}{\rightarrow} CH_4 \tag{3}$$

It has been proposed that the rate determining step of the FT synthesis is the hydrogenation of one of the surface carbon species shown in equation six, where k_1, k_2 or k_3 are rate constants. Equations 1 and 2 are assumed to be at equilibrium. The rate of product formation is:

$$R(P) = k_x \theta_C \theta_H{}^x \tag{4}$$

where x is the number of H in in the CH_x species formed during the rate determining step. Under typical FT conditions, it is assumed that $\theta_C \approx 1$ and θ_H is determined by the equilibrium constant (K_H) for dissociative chemisorption of H_2 and the competition for vacant sites by CO and H_2. The surface coverage of H is given by:

$$\theta_H = K_H^{1/2} P_{H_2}^{1/2} (1 + bP_{CO})^{-1/2} \tag{5}$$

and the rate of product formation is equal to:

$$R(P) = k_1 K_H^{1/2} P_{H_2}^{1/2} (1 + bP_{CO})^{-1/2} \tag{6}$$

where x and θ_C from equation 4 are both equal to 1. It is generally accepted that $k_{1,H} > k_{1,D}$ and $K_D > K_H$. Switching from D_2 to H_2 would effect both k_1 and $K_{H(D)}$ in opposite directions so wether there is an inverse, normal or no isotope effect would depend on the magnitude of change in k_1 and $K_{H(D)}$.

UC/B

In this reporting period, we continued our X-ray absorption spectroscopic (XAS) studies at the Stanford Synchrotron Radiation Laboratory (SSRL) with emphasis on Fe K-edge measurements on our standard samples and on a series of fresh and used Fe-Si catalysts provided by Dr. Burtron A. Davis at the Center for Applied Energy Research (CAER) of University of Kentucky. We measured the XAS spectra of standard compounds: Fe_2O_3, Fe_3O_4, FeO, $ZnFe_2O_4$ and FexC. We also investigated the *in-situ* reduction and carburization behavior of Fe_2O_3 in synthesis gas. In addition, we measured five samples from CAER that consisted of unpromoted precipitated Fe oxides (RJO 249) and its samples used for various lengths of time for FTS (RJO282C, D, G and J).

We have also investigated the isotopic effects using synthesis gases of $D_2/CO/N_2$ (62/31/7) and $H_2/CO/N_2$ (62/31/7) on an Fe-Zn catalyst (Zn/Fe=0.1, K/M=0.02, Cu/Fe=0.01) at 235°C and 21.4 atm. Compared with the results using the synthesis gas of $H_2/CO/N_2$, lower methane and CO_2 selectivities and a higher selectivity to C_{5+} were obtained with $D_2/CO/N_2$.

Inverse isotopic effects for CO conversion rate and hydrocarbon formation rate and a normal isotopic effect for CO_2 formation were observed when D_2 was used instead of H_2. The k_H/k_D ratio for hydrocarbon formation decreased with increasing CO conversion and with increasing carbon number, suggesting that isotopic effects were more evident for the formation of hydrocarbons with higher molecular weight, and for the formation of paraffins than for olefins.

In this quarter, an additional reaction pathway was studied for the Co-catalyzed FTS. We assumed that both H_2 and H_2O promote the dissociation of adsorbed CO, which controls the CO consumption rate. Kinetic studies were carried out by running FTS reaction on a 21.9 wt.% Co/SiO_2 catalyst at 200°C. The reactants, CO (2.3-8.7 atm), H_2 (9.3-25.0 atm), and H_2O (0.5-2.0 atm) in different molar ratios, were introduced into the reactor separately. CO conversion and selectivities of primary hydrocarbons (up to C_{12}) were measured at steady states. The CO consumption rate data along with those obtained from the previous kinetic run were fitted to rate expressions on the basis of our proposed mechanisms with multivariable non-linear regression.

H_2/D_2 isotope effects during FTS were studied by running the reactions with both CO/H_2 and CO/D_2 over a 21.9 wt.% Co/SiO_2 catalyst at 200°C and 20 atm. The kinetic isotope effects for CO consumption and for individual hydrocarbons C_1-C_7 were obtained by comparing the corresponding reaction rates with H_2 and D_2. Inverse kinetic isotope effects were obtained for CO consumption ($k_H/k_D = 0.8$) when the CO conversions were between 10% and 40%. The results showed that the isotope effects (k_H/k_D) were generally inverse for paraffins whereas normal for olefins at low conversions when the effect of secondary reactions could be neglected. These isotope effects resulted from a combination of kinetic and equilibrium isotopic effects which may be associated with individual elementary steps.

Task 1. Iron Catalyst Preparation

The objective of this task is to produce robust intermediate- and high-α catalysts.

Task 2. Catalyst Testing

The objective of this task is to obtain catalyst performance on the catalysts prepared in Task 1.

A. Deuterium Isotope Effects with a Precipitated Iron Catalyst in Slurry Phase Fischer-Tropsch Synthesis

The impact of deuterium on the Fischer-Tropsch (FT) synthesis was studied with a precipitated iron catalyst in the slurry phase. As indicated in the summary, the data will provide design data for slurry reactors and separators. Deuterium has been used by several research groups to better understand the mechanism of CO hydrogenation. Inverse ($k_H/k_D < 1$), normal ($k_H/k_D > 1$) and no isotope effect ($k_H/k_D = 1$) have been reported (1). The conflicting results are thought to arise because rate of reaction is a combination of kinetic and equilibrium factors (2).

Experimental

Precipitated iron catalyst (100Fe/4.6Si/1.44K, atomic basis) (5g) was added to 310 g of Polywax 3000 (Petrolite, average M.W.=3000) which had been melted at 130^{O}C in a one liter CSTR. The catalyst was activated with CO as follows. The reactor stirrer was set at 750 rpm, CO flow was started at 25 slph, the pressure was increased to 175 psig and the temperature was increased to 270^{O}C at 2^{O}C/min. These conditions were maintained for 24 hours and then the CO flow was lowered to 9.55 slph and D_2 flow was started at 6.52 slph. Fischer-Tropsch conditions were: whsv=5.0 sl h^{-1} g-Fe^{-1}, D_2/CO=0.67, 270^{O}C and 175 psig. Periodically D_2 was stopped and H_2 was used. The time on stream for each gas is shown in Table 1.

Table 1 Time on Stream for D_2 and H_2	
Time on stream (h)	**Gas**
0 - 137	D_2
138 - 330	H_2
331 - 384	D_2
385 - 859	H_2

H_2 or D_2 and CO flow rates were controlled by two mass flow controllers (Brooks Instruments) with the resulting synthesis gas composition regulated by adjusting the flow rate of the appropriate gas. The synthesis gas, after passing through a 2 L mixing vessel, was delivered to the catalyst slurry through a dip tube that extended to below the impeller blade. The reactor effluent exited the reactor and passed sequentially through two traps maintained at 60^{O}C and 0^{O}C. Accumulated reactor wax was removed daily through a tube fitted with a porous metal filter (0.5 μm) and collected in a 200^{O}C trap . Uncondensed effluent was fed to a multichannel on-line refinery gas analyzer (Hewlett Packard Quad Series Micro GC) for determination of CO, H_2, D_2, CO_2, CH_4 and C_2 - C_8 alkanes and alkenes.

After 130 hours of FTS with D_2, 25 ml of a solution of 5.0 g of 1-heptene (C_7H_{14}, Aldrich) and 5.0 g of 1-octene (C_8H_{16}, Aldrich) in decalin (Aldrich) were pumped into the reactor over a two hour period with a LDC/Milton Roy pump. Liquid samples were collected four hours and 24 hours after pumping the alkene mixture. Liquid samples will be analyzed by GC-MS to determine the relative rates of alkene isomerization and hydrogenation.

Results and Discussion

Through the first 137 hours of FTS with D_2 , there was an induction period in which the syngas conversion gradually increased to 86% (Figure 1). During this time, 90.8 g of deuterated liquid hydrocarbon products were collected. The use of Polywax 3000 polyethylene, low vapor pressure under reaction conditions, as a slurry medium prevented the condensed liquid products from being contaminated with hydrogen containing compounds from the initial slurry medium.

During slurry phase FTS, a significant amount of product is held-up in the reactor which can influence the product distribution. Samples collected after D_2 was stopped will be analyzed by GC-MS to determine the reactor hold-up time of alkanes and alkenes as a function of carbon number.

Syngas conversion was stable after about 137 hours on stream and at this time D_2 was stopped and H_2 was started. There was a rapid decease in syngas conversion from 86% to 78% during the first 24 hours after H_2 was started and during the next 200 hours (TOS=330 h), the syngas conversion gradually decreased to 74% (Figure 1). After this time, H_2 was stopped and D_2 was restarted. Switching back to D_2 caused the syngas convesion to increase to 83% within 24 hours of the change. Conversion remained constant for 48 hours and then H_2 was restarted. Once again the syngas conversion rapidly decreased after D_2 was stopped and H_2 was started.

The FT rate responded similarly as the syngas conversion (Figure2); however, the water-gas shift (WGS) rates increased only slightly after changes from D_2 to H_2 were made (Figure 3). The FT and WGS rates are defined as as follows:

$$r_{FT} = r_{CO} - r_{CO_2} \quad (1)$$

$$r_{WGS} = r_{CO_2} \quad (2)$$

where r_{CO} is the rate of CO conversion and r_{CO_2} is the rate of CO_2 formation. When the switch from H_2 to D_2 was made after 330 hours on stream, the FT rate increased from 0.054 to 0.064 mol h^{-1} g-Fe^{-1} and the WGS rate increased from approximately 0.044 to 0.047 mol h^{-1} g-Fe^{-1}. There was significant variance in the WGS shift data (Figure 3); however, it is clear that the WGS rate decreased after the initial switch from D_2 to H_2 was made and increased when the switch from H_2 to D_2 was made. The isotope effect (k_H/k_D) observed for the FT rate was 0.85 and approximately 0.93 for the WGS rate.

There was also an isotope effect observed for CH_4 selectivity and alkene selectivity. CH_4 selectivity is defined as follows:

$$CH_4 sel = \frac{r_{CH_4}}{r_{FT}} x100 \quad (3)$$

where r_{CH_4} is the rate of CH_4 production. Figure 4 shows that the methane selectivity increased steadily from approximately 5% to 20% throughout the run. A decrease in the CH_4 selectivity from 9.0% to 7.4% was observed when H_2 was switched to D_2 after 330 hours on stream. This is a relative decrease of 18%. When D_2 was switched back to H_2 the CH_4 selectivity increased to 9.7%. Similar trends were observed for C_2, C_3 and C_4 alkene selectivity (Figure 5) which is defined as the molar ratio, alkene/(alkene+alkane). Initially the alkene selectivity decreased as the syngas conversion increased during the first 137 hours on stream. After the conversion stabilized, the C_2, C_3 and C_4 alkene selectivity were 0.11, 0.69, and 0.74, respectively. Switching from H_2 to D_2 caused the C_2, C_3 and C_4 alkene selectivity to increase to 0.19, 0.73, and 0.77, respectively. This corresponds to relative increases of 73%, 6% and 4% for the C_2, C_3 and C_4 alkene selectivity, respectively.

The isotope effect with deuterium is probably the combination of equilibrium and kinetic effects (2-4). The proposed steps for the hydrogenation of carbon monoxide are:

$$H_2 \overset{K_{H'}}{\leftrightarrows} (H_2)_s \overset{K_{H''}}{\leftrightarrows} 2H_s \tag{4}$$

$$CO \overset{K_{CO'}}{\leftrightarrows} CO_s \overset{K_{CO''}}{\leftrightarrows} C_s + Os \tag{5}$$

$$C_s + H_s \overset{k_1}{\leftrightarrows} CH_s \overset{k_2}{\leftrightarrows} CH_{2,s} \overset{k_3}{\leftrightarrows} CH_{3,s} \overset{k_4}{\rightarrow} CH_4 \tag{6}$$

It has been proposed that the rate determining step of the FT synthesis is the hydrogenation of one of the surface carbon species shown in equation six, where k_1, k_2 or k_3 are rate constants (2). Equations 4 and 5 are assumed to be at equilibrium. The rate of product formation is:

$$R(P) = k_x \theta_C \theta_H{}^x \tag{7}$$

where x is the number of H in in the CH_x species formed during the rate determining step. Under typical FT conditions, it is assumed that $\theta_C \approx 1$ and θ_H is determined by the equilibrium constant

(K_H) for dissociative chemisorption of H_2 and the competition for vacant sites by CO and H_2. The surface coverage of H is given by:

$$\theta_H = K_H^{1/2} P_{H_2}^{1/2} (1 + bP_{CO})^{-1/2} \quad (8)$$

and the rate of product formation is equal to:

$$R(P) = k_1 K_H^{1/2} P_{H_2}^{1/2} (1 + bP_{CO})^{-1/2} \quad (9)$$

where x and θ_C from equation 7 are both equal to 1(2). It is generally accepted that $k_{1,H} > k_{1,D}$ and $K_D > K_H$. Switching from D_2 to H_2 would effect both k_1 and $K_{H(D)}$ in opposite directions so wether there is an inverse, normal or no isotope effect would depend on the magnitude of change in k_1 and $K_{H(D)}$.

References

1. A. Raje and B. H. Davis. Fischer-Tropsch Synthesis. Mechanism Studies Using Isotopes. In *Catalysis*; J. J. Spivey, Ed.; The Royal Society of Chemistry; 1996; Vol. 12.
2. T. P. Wilson, *J. Catal.*, 1979, **60**, 167.
3. C. S. Kellner and A. T. Bell, *J. Catal.*, 1981, **67**, 175.
4. M. A. Logan and G. A. Somorjai, *J. Catal.*, 1985, **95**, 317.

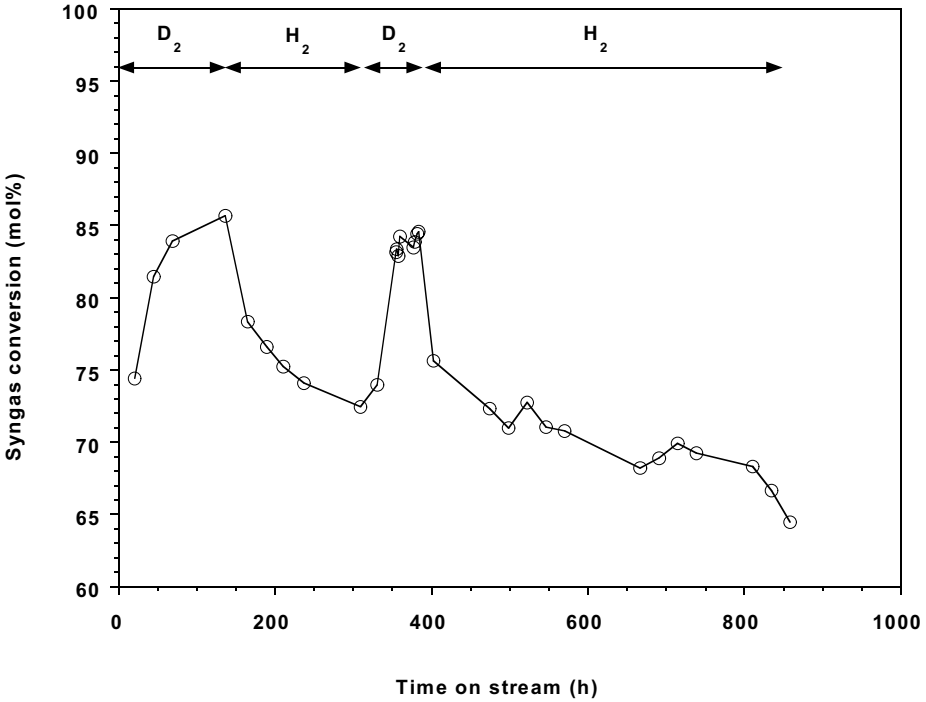

Figure 1. Syngas conversion as a function of time on stream.

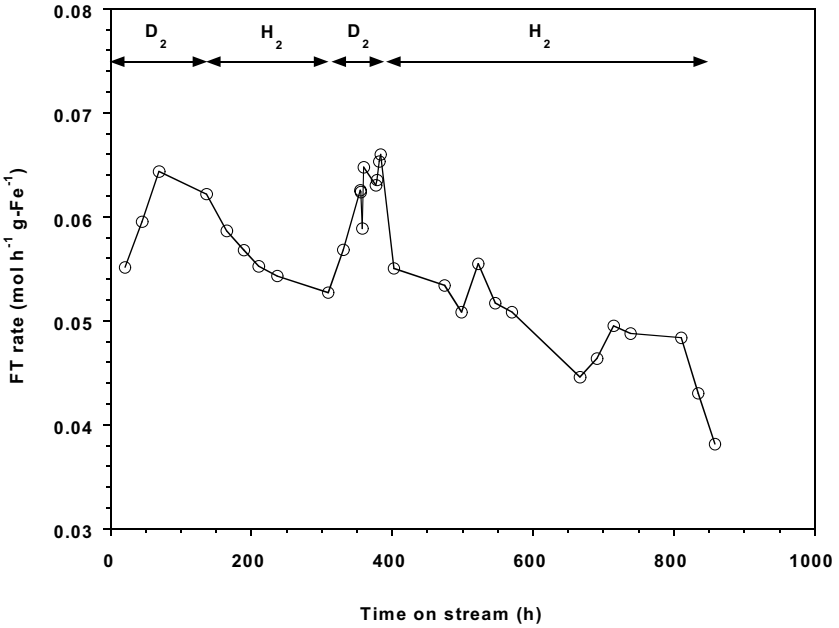

Figure 2. Effect of deuterium on FT rate.

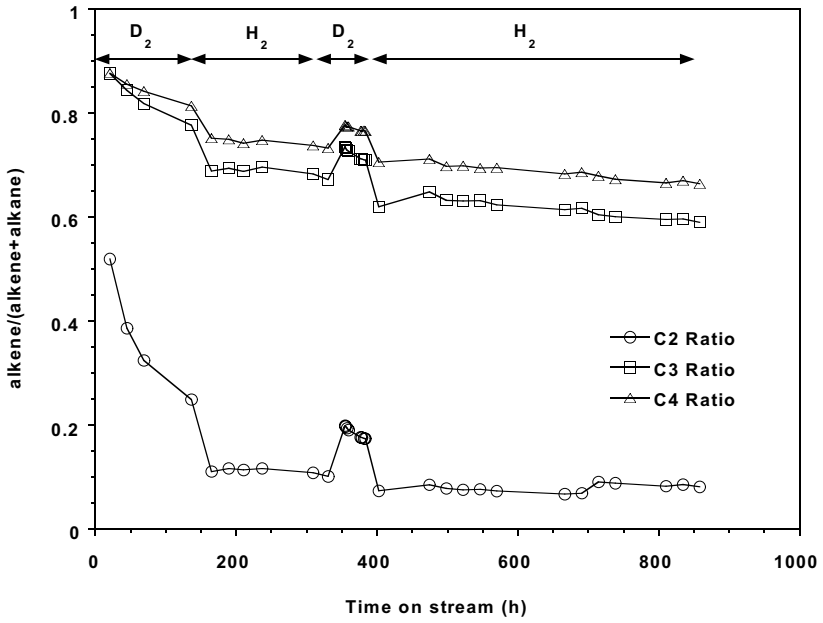

Figure 3. Effect of deuterium on C_2, C_3 and C_4 alkene selectivity.

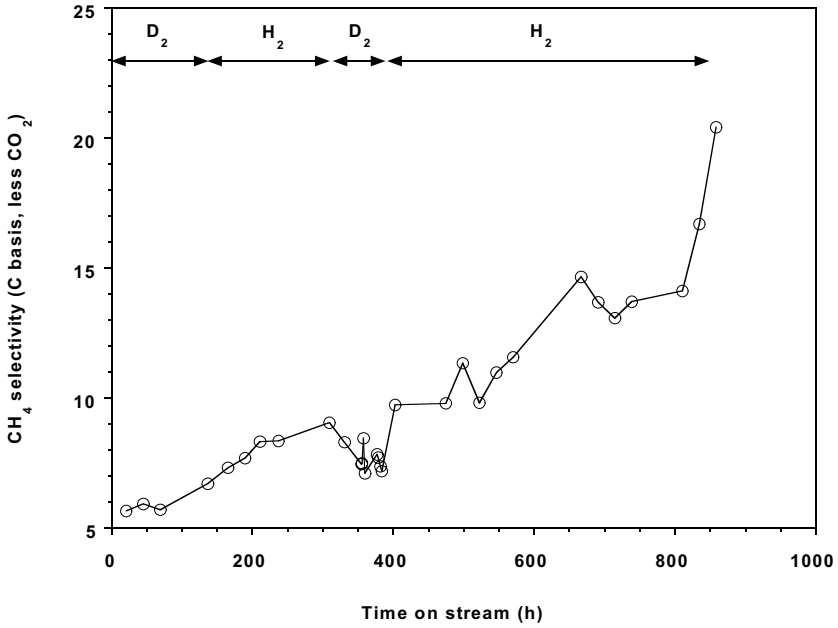

Figure 4. Effect of deuterium on CH_4 selectivity.

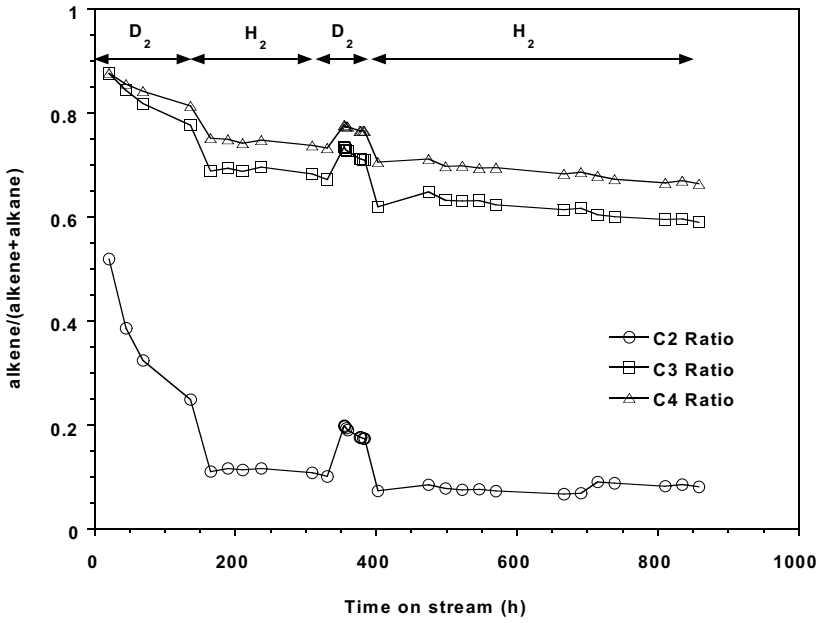

Figure 5. Effect of deuterium on C_2, C_3 and C_4 alkene selectivity.

B. Reactor Engineering — CSTR Mixing Study

In a CSTR slurry reactor, the concentration distribution of solid catalyst in the reactor liquid significantly affects the reaction conversion. The catalyst dispersion is related to the liquid rotation speed under agitation. A cold mold test of our CSTR reactor (1 liter) was conducted in the absence of baffle to examine how liquid speed responds to agitation speed. About 300 gram of C30 oil was used as medium with a small ball (2 mm diameter) placed on liquid surface to measure the liquid rotation speed. The mixing apparatus and dimensions are shown schematically in Figure 1.

It was observed that the ball did not reside on a radial position close to the tank wall as expected. Instead, the orbit of the ball was relatively irregular, spanning from the agitator shaft and inner tank wall. Therefore, the measured liquid speed was interpreted as the average speed in the tank, rather than at a fixed radial position. Figure 2 shows the measured liquid speed vs. agitation speed, both in terms of rpm.

The lowest agitation speed used in this test was 610 rpm, which corresponds to a mixing Reynold's number of 2200. Thus all the mixing tests are under turbulent conditions. According to an empirical correlation available in literature for large agitation tank, the distribution of linear liquid velocity (cm/s) and liquid rotation speed (rpm) can be calculated as shown in Figure 3 for agitation speed of 1040 rpm. The measured liquid speed is equivalent to that at the radial position of r/R = 0.47. This value also applies to the other tests. It should be noted that the literature correlation is for large agitation tanks and when liquid velocity is not a function of axial position. In our test, the ball stays on liquid surface which is actually a convex and the convexity changes with agitation speed. In the absence of the baffle, the liquid rotation approaches that of the stirrer. Even with the baffles, the liquid rotation should be greater than half that of the stirrer.

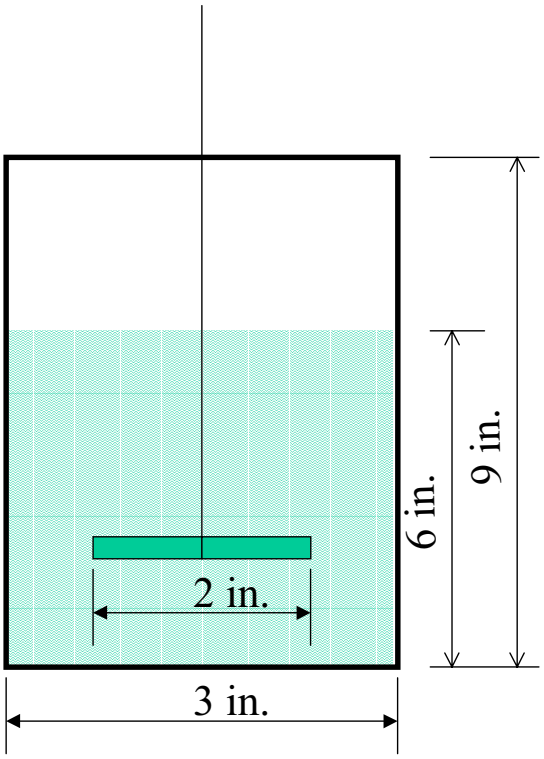

Figure 1 Agitation Apparatus

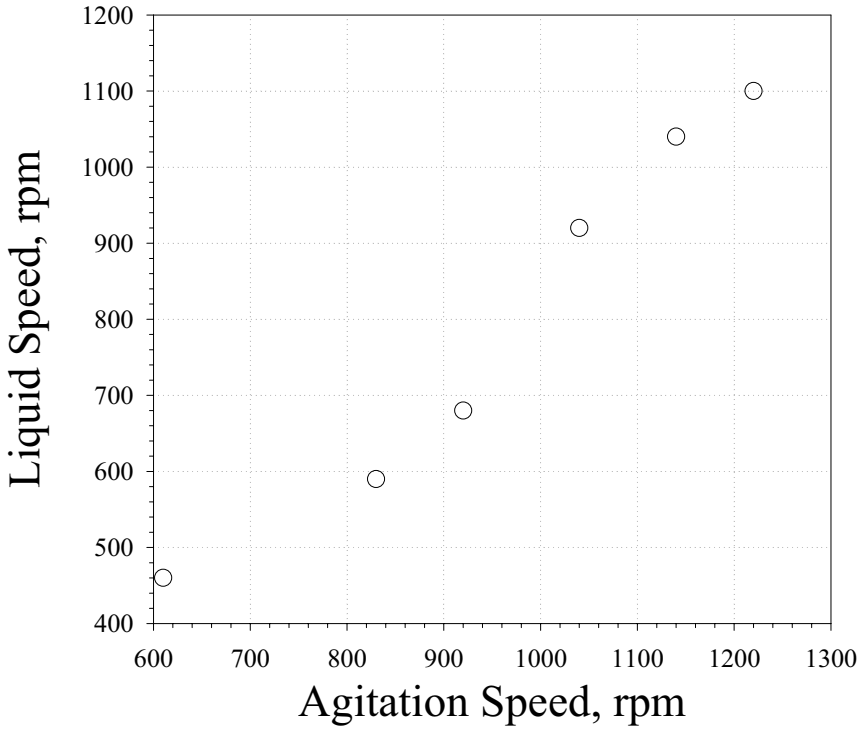

Figure 2 Measured liquid speed vs. agitation speed

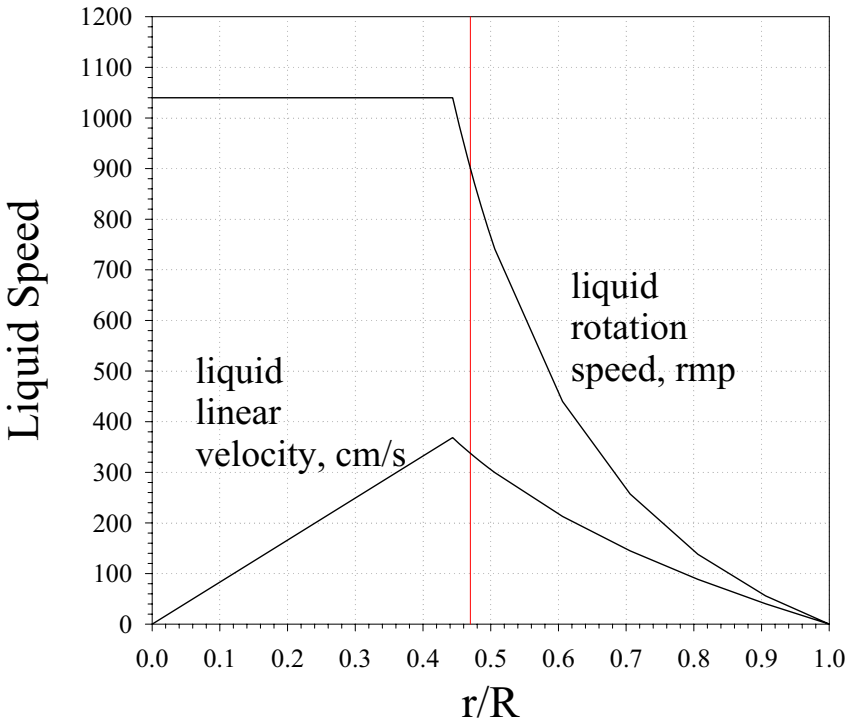

Figure 3 Liquid speed distribution in the tank

Task 3. Catalyst Characterization

The objective of this task is to obtain characterization data of the prepared catalysts using routine and selected techniques.

No scheduled or further activity to report.

Task 4. Wax/Catalyst Separation

The objective of this task is to develop techniques for the separation of catalysts from FT reactor slurries.

A meeting with Pall officials is scheduled for November 8, 1999. It is anticipated that a joint research project will be defined during this meeting. This follows a previous meeting with Pall, the CAER P.I. and two companies who were interested in separations.

Task 5. Oxygenates

The objective of this task is to obtain a better understanding of the factors that affects catalyst selectivity toward oxygenates for iron-based Fischer-Tropsch catalsyts.

No scheduled or further activity to report.

Task 6. Literature Review of Prior Fischer-Tropsch Synthesis with Co Catalysts

The objective of this task is to prepare a critical review of prior work on cobalt Fischer-Tropsch catalysts.

Literature is being compiled to augment the current report on this task.

Task 7. Co Catalyst Preparation

The objective of this task is to prepare a limited number of cobalt-based Fischer-Tropsch catalysts that can be used to obtain baseline data on cobalt-based Fischer-Tropsch synthesis.

Supports have been obtained as well as those prepared at the CAER to sue to prepare supported catalysts.

Task 8. Cobalt Catalyst Testing for Activity and Kinetic Rate Correlations

The objective of this task is to conduct initial screening of the cobalt catalysts prepared in Task7 to select three baseline catalysts that will then be used to generate a data base on the performance of cobalt-based Fischer-Tropsch catalysts in slurry reactors.

A run in the CSTR has been completed that allows the comparison of the productivity of a cobalt catalyst in a CSTR and a supercritical fixed-bed reactor. To a first approximation, the productivity/g catalyst is similar in the two reactors.

A. The CSTR studies of Co(10)/B(x)/TiO_2 Fischer-Tropsch catalysts

1. Reaction system

A 1-liter autoclaver, operated as a continuous stirred tank reactor (CSTR), was used for the slurry FTS reactions. Analysis of the gaseous, liquid, and solid (at room temperature) products was conducted both on and off line using a variety of gas chromatographs.

2. Procedure

The catalysts used were 10 wt% Co/TiO_2 and 10 wt% Co/ 0.05% B/TiO_2, prepared by incipient wetness impregnation. Catalyst (about 15 g) was reduced *ex-situ* with hydrogen at 300ºC for 16 h and transferred under the protection of helium to CSTR to mix with 300 g of melted P.W. 3000. The catalyst was then reduced *in-situ* in the CSTR; the hydrogen was introduced to reactor at atmospheric pressure with a flow rate of 30 $NLh^{-1}gcat.^{-1}$ (25ºC, 0.1 mPa). The reactor temperature was increased to 280ºC at a rate 120ºC h^{-1} and maintained at this activation condition for 24 h. After the activation period, the reactor temperature was decreased to 210ºC and synthesis gas was then introduced. During the entire run the reactor temperature was 230ºC, the pressure was 350 psig, and the stirring speed was maintained at 750 rpm.

The space velocity of the synthesis gas was varied from 1 to 5 NL h^{-1} $gcat.^{-1}$ at a constant H_2/CO ratio of 2. Afterwards, the H_2/CO ratio synthesis gas was varied from 2 to 5 at a constant space velocity of 2 NL $h^{-1}gcat.^{-1}$. The conversion of carbon monoxide and hydrogen and the formation of products were measured during a period of 24 h at each condition.

3. Results

The attached figures show that synthesis gas conversion, methane selectivity and hydrocarbon production rate varied with space velocity and the H_2/CO ratio for two catalysts.

Synthesis gas conversion for two catalysts is shown in Figure 1. The synthesis gas conversion was found to increase with decreasing space velocity. At the higher space velocity (SV>4), the two catalysts showed very similar synthesis gas conversion; at low space velocity (SV<4), the catalyst with 0.05 % B showed a slightly higher conversion.

Figure 2 shows the hydrocarbon production rate as a function of reciprocal flow rate. For the catalyst with 0.05% B, the hydrocarbon rate increased almost linearly with increasing space velocity. For B-free catalyst, the hydrocarbon rate increased first and then kept a constant of 2.0 g/gcat./h with increasing space velocity; however, the difference between the two runs is small.

From Figure 3, we find the methane fraction of the hydrocarbons increased with increasing space velocity. For all space velocities, the catalyst with 0.05% B showed higher methane selectivity.

For two catalysts, the effects of H_2/CO ratio on conversion and methane selectivity are very similar (Figures 4 and 5). Increasing the ratio of H_2/CO resulted in: (i) synthesis gas conversion increased first and then decreased and reached a maximum at the H_2/CO of 4; (ii) methane selectivity increased almost linearly.

In summary, the presence of boron produced only minor changes on the properties of the cobalt catalyst. In earlier studies, it was shown that the presence of boron made the catalyst less susceptible to poisoning by sulfur.

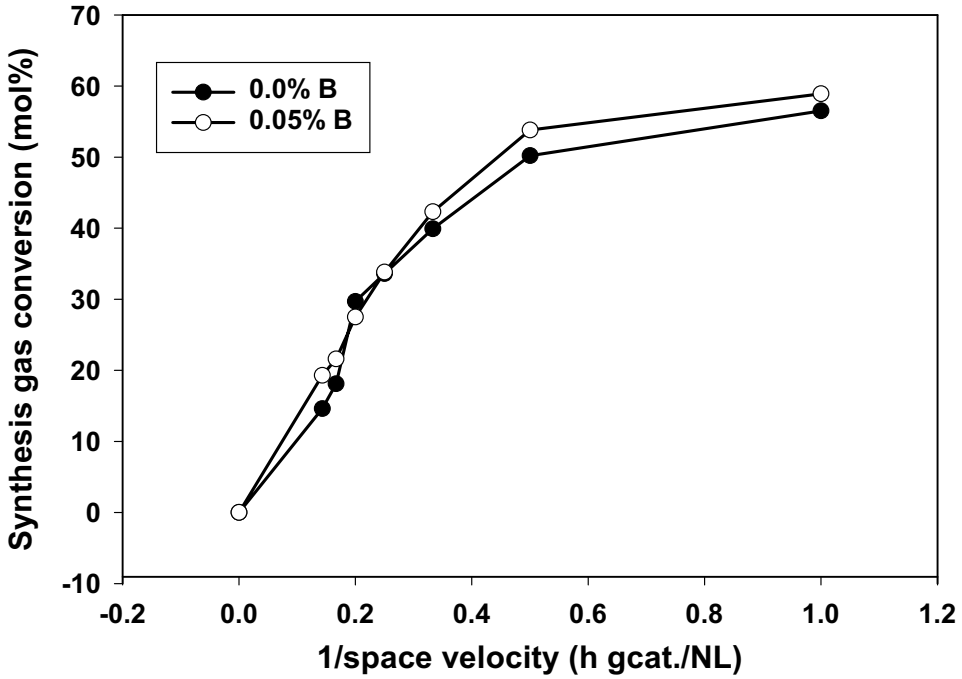

Figure 1. Synthesis gas conversion as a function of reciprocal flow rate

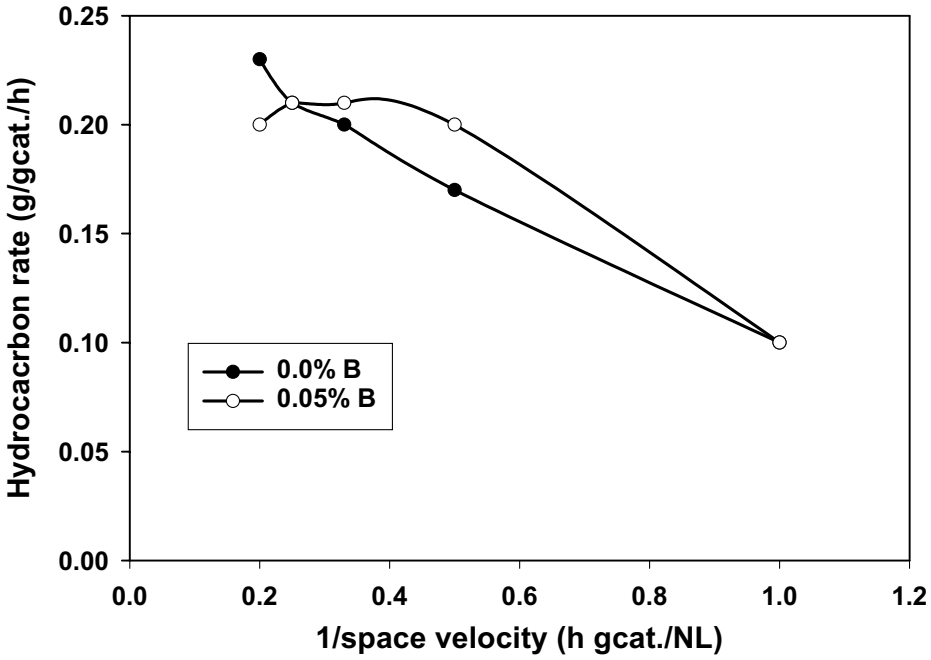

Figure 2. Hydrocarbon production rate aas a function of reciprocal flow rate

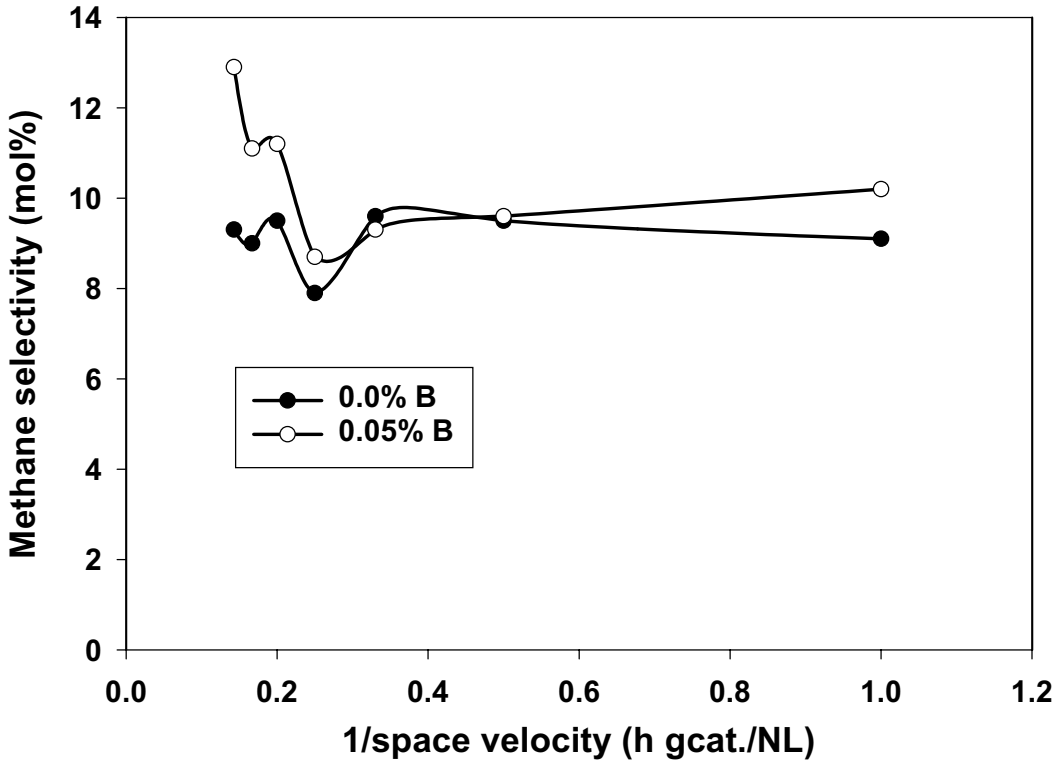

Figure 3. Methane selectivity vs reciprocal flow rate

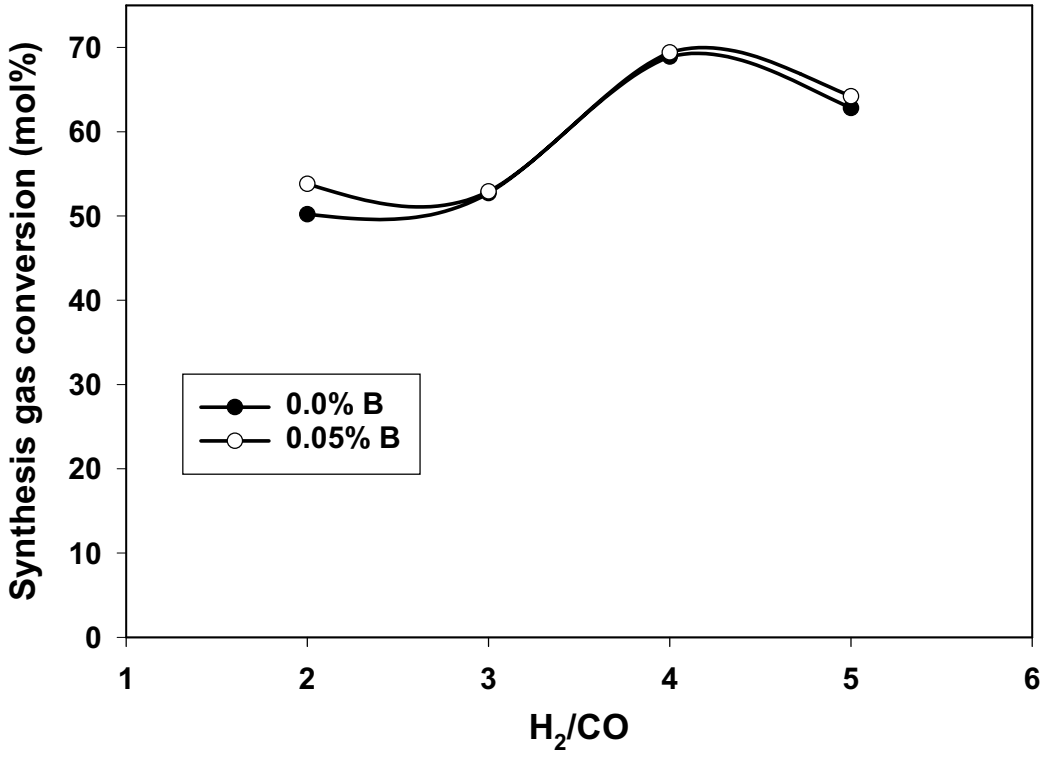

Figure 4. Synthesis gas conversion vs ratio of H_2 to CO (at SV=2 NL/gcat./h)

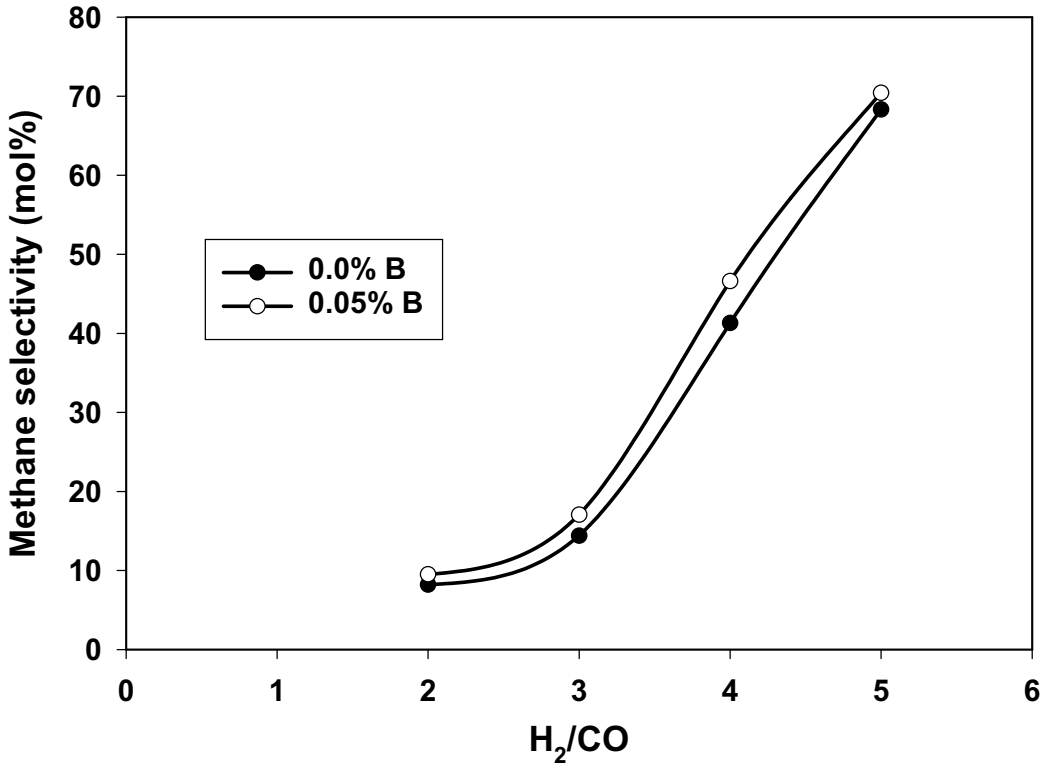

Figure 5. Methane selectivity vs ratio of H_2 to CO (at SV=2 NL/gcat./h)

B. Study of supercritical phase Fischer-Tropsch synthesis

1. Introduction:

Fischer-Tropsch synthesis has been studied extensively in both gas and liquid phase reaction media, in which fixed-bed and CSTR or bubble column slurry phase reactors were used respectively. Gas phase reactions may exhibit higher initial reaction rates but also is inevitably accompanied by local overheating of the catalyst surfaces as well as by the deposition of heavy wax in catalyst pores. Local overheating of the catalyst and the plugging of the pores of the catalyst may lead to deactivation of the catalyst and also to an increase in methane selectivity. Liquid phase reactions have superior heat removal capabilities when compared to gas phase reactions and are, therefore, able to maintain a relatively constant reaction temperature throughout the whole reactor. Another advantage of liquid phase synthesis is that the high molecular weight products are more soluble in the liquid media compared to gas phase reaction media. However, the diffusion of synthesis gas into the pores of the catalysts may be slower in the slurry phase so that the overall reaction rate may therefore be lower. In addition, problems may arise as the accumulation of high molecular weight products in the reactor during the operation, and the *in situ* separation of fine catalyst particles from the heavy products remain to be solved for liquid phase reaction. The ideal FT synthesis medium would therefore be one with gas-like transport properties and liquid like heat capacity and solubility characteristics. Such a desired combination of fluid properties can possibly be obtained by conducting the Fischer-Tropsch synthesis in a supercritical reaction media.

The critical temperature of a fluid is the highest temperature at which liquid and vapor can exist together. The pressure at which condensation of vapor to liquid occurs when the temperature is equal to the critical temperature is the critical pressure. At temperatures above the critical temperature a fluid cannot undergo a transition to a liquid phase, regardless of he pressure applied. A fluid is said to be supercritical when its temperature and pressure exceed the temperature and pressure at the critical point. Supercritical fluid (SCF) are attractive media for chemical reactions because of their unique properties such as viscosity, diffusivity, density and

solubility. Many of the physical and transport properties of an SCF are intermediate between those of a liquid or a gas. Changing the pressure near the critical region can tune the density and transport properties of a fluid to obtain unique fluid properties (e.g., gas-like transport properties or liquid-like solvent power), which offer certain advantages in heterogenous catalysis reactions. Specific to the Fischer-Tropsch synthesis reaction, it seems SCF can possibly in situ extract the heavy hydrocarbons from the catalyst pores, thereby extending catalyst lifetime. The diffusion of reactant, hydrogen and carbon monoxide, as well as both primary and secondary hydrocarbon products could also be effected by SCF and favorably affect reaction rate and selectivity.

Studies on Fischer-Tropsch synthesis in supercritical media have, to date, been done primarily by three groups of scientists. Fujimoto's group is a pioneer in the area, an excellent job was done by applying the idea to Fischer-Tropsch synthesis; however, the lack of steady-state data made the results less convincing than desired. Bukur's group did steady state work; nevertheless, by using propane as the supercritical media, the density of the solvent is not high enough to attain the optimum solubility properties. Subramaniam's group did the pressure tuning work using hexane as the solvent; still, different syngas partial pressures and residence times were used to compare the activity and selectivity. Therefore, too many variables were introduced to draw solid conclusions.

Steady-state supercritical Fischer-Tropsch synthesis was studied in our work using a fixed-bed reactor and an unpromoted Co/SiO_2 catalyst. This serves as the baseline for promoted catalyst studies. A pentane-hexane mixture was used as the supercitical solvent. Overall reactor pressure, syngas partial pressure and contact time were kept constant to obtain a valid comparison of the impact of solvent density in the catalytic activity and selectivity. Three different partial pressures of the mixture were chosen based on the density-pressure curve in order to investigate the pressure tuning effect to Fischer-Tropsch synthesis near critical region.

2. Experimental

Catalyst preparation: A 2kg batch of 15% Co/SiO2 catalyst was prepared by incipient wetness impregnation method using Davisil 644 Silica gel as support (surface area 300m^2/g, pore

volume:1.15cm^3/g, particle size 100-200mesh) and an aqueous cobalt nitrate solution for impregnation. The catalyst was dried by being suspended in air at 80^{0}C in a fluidized vessel and then calcined at 400^{0}C for 4 hrs.

Reactor diagram: A schematic of the reactor Figure 1 is the diagram used to do supercritical Fisher-Tropsch study is shown in Figure 1. Basically, it is a plug-flow reactor with a pump for adding the supercritical solvent. A characteristic of the unit is the capability of being able to be repressurize quickly after taking a liquid product for each mass balance period. Since we pump in a significant amount of solvent during the period, its removal as a liquid cause a remarkable pressure drop. The other difference between the reactor and a traditional plug-flow reactor is that we use a three heating zone furnace and the first zone filled with micro-glass beads to vaporize the solvent. We also set up two parallel sets of hot and cold traps to use for mass balance period and period between mass balance to improve the operation.

Pretreatment condition: The catalyst was reduced with mixture of hydrogen and argon. The temperature was increased to 100^{0}C during 30min and held at 100^{0}C for 30min, and after that the temperature was increased to 350^{0}C with at a rate of 1^{0}C/min, then held at 350^{0}C for 15hrs.

Reaction conditions:

Conditions	$P_{overall}$ (MPa)	P_{syngas} (Mpa) H_2:CO =2.0	$P_{solvent}$+P_{He} (MPa)	T(^{0}C)	Total Flow Rate (ml/min)	Syngas Flow Rate (ml/min)	He Flow Rate (ml/min)	Solvent Fow Rate✶ (ml/min)
1	8.0	2.0	6.0	220	200	50	150	0
2	8.0	2.0	6.0	220	200	50	100	50
3	8.0	2.0	6.0	220	200	50	62.5	87.5
4	8.0	2.0	6.0	220	200	50	0	150
✶gas phase flow rate								

3. Results and discussion:

Physical and transport properties of certain fluids change dramatically with pressure in a range around the critical pressure and at temperatures slightly higher than the critical temperature. They can be made either more gas-like or liquid-like by tuning the pressure. As to Fischer-Tropsch synthesis, the ideal situation is to find a condition where the maximum extraction of hydrocarbon products from catalyst pores can be reached to increase catalyst lifetime. However, diffusivity and viscosity of the fluid can have an impact on the degree of secondary reactions that take place on the surface of catalyst and therefore lead to changes in selectivity. Thus, different solvent and pressure tuning effects of the solvent are important to supercritical Fischer-Tropsch synthesis study.

A near optimal temperature for the cobalt catalyst being used in this study is about 220^0C; therefore, the critical temperature of the solvent chosen should be below 220^0C. Since the critical temperature for n-pentane is 197^0C and for n-hexane is 232^0C, a mixture of these two solvent can be used to obtain the maximum density. Figure 2 shows a curve of the critical temperature of pentane and hexane mixtures versus the hexane volume percentage. From Figure 2, it is calculated that 55%(V) of hexane/45%(V) of pentane mixture has the highest density whose critical temperature is under 220^0C.

In order to obtain good representative pressure points to study the tuning effect, it is necessary to have an idea of how density changes with pressure near the critical region. Figure 3 is the density of 55%(V) n-hexane and 45%(V) n-pentane mixture versus pressure curve between 1-15MPa at 220^0C (a Hysys 2.1 process simulator was used to calculate the density data). Partial pressures of 2.0MPa, 3.5MPa and 6.0MPa of the mixture were chosen to represent the gas-like, supercritical and liquid like conditions, respectively. Helium was used as a balancing gas to keep the overall pressure and residence time constant. Altogether, four conditions were studied; this included no added solvent and three different solvent partial pressures. After taking a liquid sample, helium was charged to the cold trap to make up the pressure drop. Hot and cold traps

temperatures were controlled at 160^0C and 0^0C respectively. Mass balance time of each sample was around 2 hrs.

Exit flow rate and molar percentage of the components of the gas was used to calculate CO conversion. Normalized exit flow rate was obtained by converting for the increase of flow rate caused by condensation of solvent in the cold trap and the amount of solvent in the exit gas phase. The rate of volume decrease of the reactor-collector may increase rapidly enough for this correction to make a large change in the measured conversion.

CO conversion versus time on stream data are shown in Figure 4. It can be concluded from Figure 4 that the supercitical phase Fischer-Tropsch synthesis significantly alters the total conversion and inhibit the deactivation of the catalyst. As a matter of fact, introducing only 2.0MPa of the pentane-hexane mixture to the reactor increased the CO conversion from 27% to 46%. The mixture at this pressure is not at its supercritical state; however, the density of the reaction media is much higher than condition 1 in which only helium was the balancing gas. Therefore, the solubility of the hydrocarbon in reaction media was increased, and it is concluded that the catalyst pores contained less liquid and more active sites were available which leads to the increase of the CO conversion. After 3.5MPa of pentane-hexane mixture was fed into the reactor (condition 3), the reaction media should be in the supercitical phase. The density is much higher than that in condition 2, causing the solubility to increase significantly, while, the diffusivity of reactant and the product is reasonably fast; therefore, the highest CO conversion was obtained. When the partial pressure of pentane-hexane mixture reached 6.0MPa (condition 4), the density of the mixture is more liquid-like and the maximum extraction of the heavy wax product occurs; however, the diffusivity of the media is also more liquid like. This may have limited the Fischer-Tropsch reaction and hence slightly lower CO conversion was observed. Several steady-state data were obtained for each condition and the reproducibility is good as shown by the data in Figure 4 for repeating the measurements at each condition. Throughout the period that solvent was introduced into the reactor, the deactivation is rather negligible. After switching back to the condition 1 in which no solvent was introduced, the CO conversion

decreased to 40% from 49% at condition 2. The deactivation was rapid at this condition and conversion decreased to 16.0% in only 33 hrs.

Since the analysis of the liquid product is not complete, the α value of the reaction has not been defined. Nevertheless, the selectivities of methane and CO_2 were calculated and the results are interesting. Figures 5 and 6 show the selectivity of methane and carbon dioxide with time on stream, respectively. It can be seen that methane selectivity decreased dramatically with the introduction of solvent into the reactor system. The higher the partial pressure of the pentane-hexane mixture, the lower the methane selectivity. The formation of CO_2, while small, and parallel that of methane.

4. Conclusion

Steady-state supercritical Fischer-Tropsch synthesis was studied using a fixed-bed reactor and a Co/SiO_2 catalyst. A pentane-hexane mixture was used as the supercitical solvent. Overall reactor pressure, syngas partial pressure and contact time were kept constant to obtain valid comparisons.

Three different partial pressure points of the mixture were chosen based on the density-pressure curve to investigate the pressure tuning effect for Fischer-Tropsch synthesis near critical region. It was found that supercitical phase Fischer-Tropsch synthesis can significantly inhibit the deactivation of catalyst, presumably due to the extraction of heavy hydrocarbon products from catalyst pores and possibly improving the heat transfer in plug-flow reactor. The highest CO conversion was obtained when the solvent partial pressure is just above its critical pressure compared to its more gas-like or liquid- like state. Reproducible data were obtained by repeating the measurements.

Methane and carbon dioxide selectivity decreased dramatically with an increase of pentane-hexane partial pressure. The selectivity of reaction and α value of different conditions will be defined in future work.

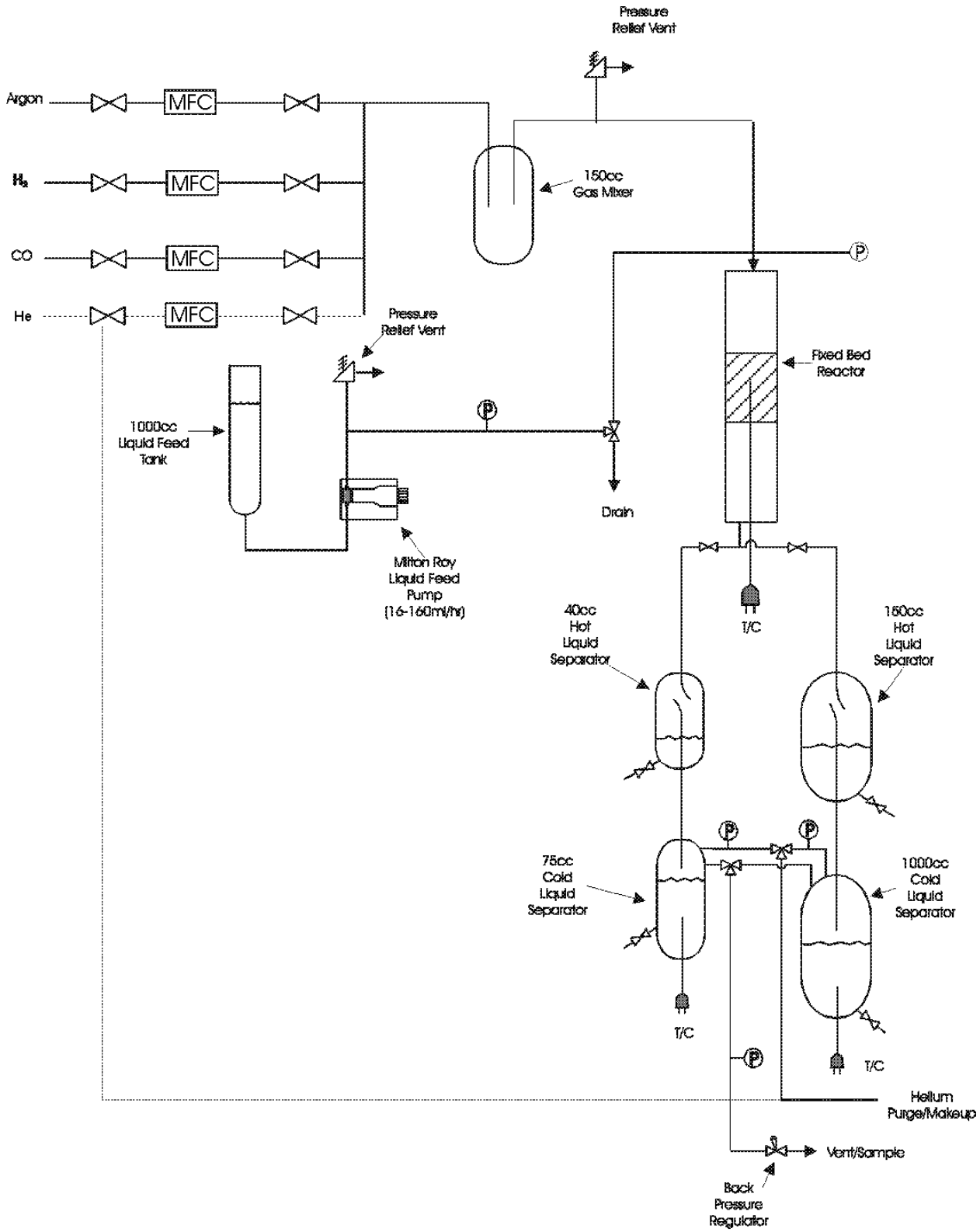

Figure 1. Supercritical FT Reactor-Flow Diagram

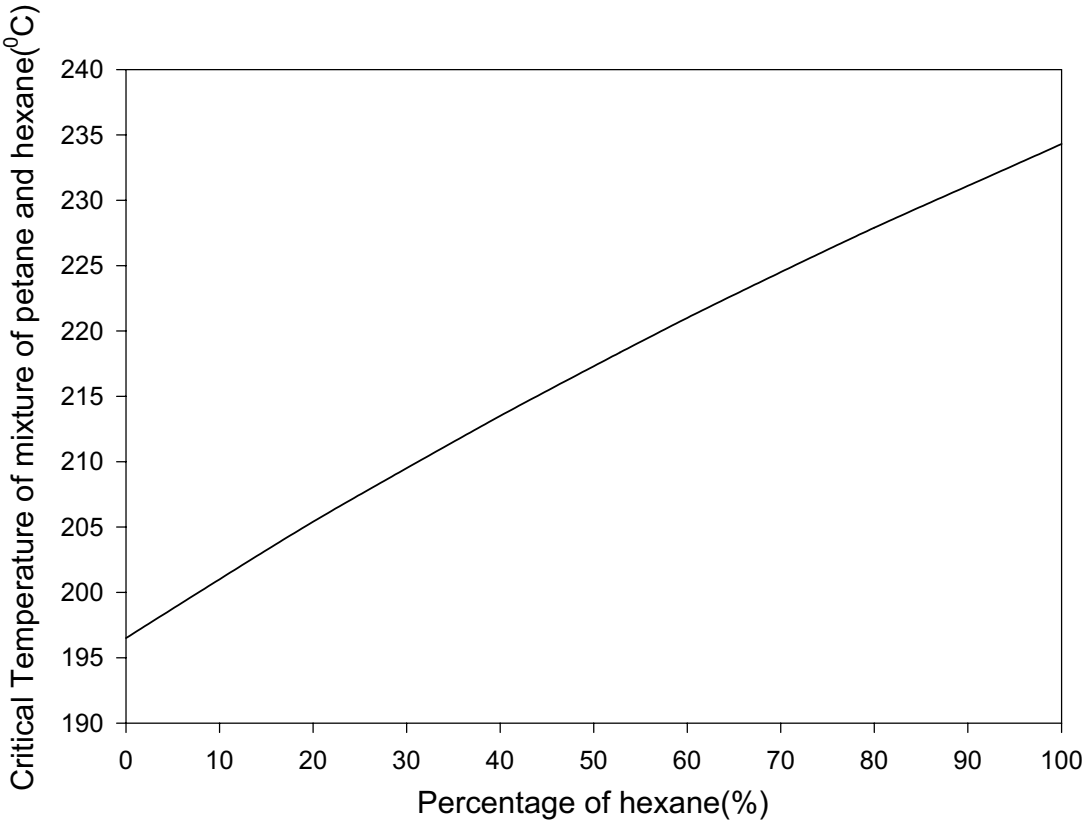

Figure 2. Critical temperature of pentane and hexane mixture with hexane percentage.

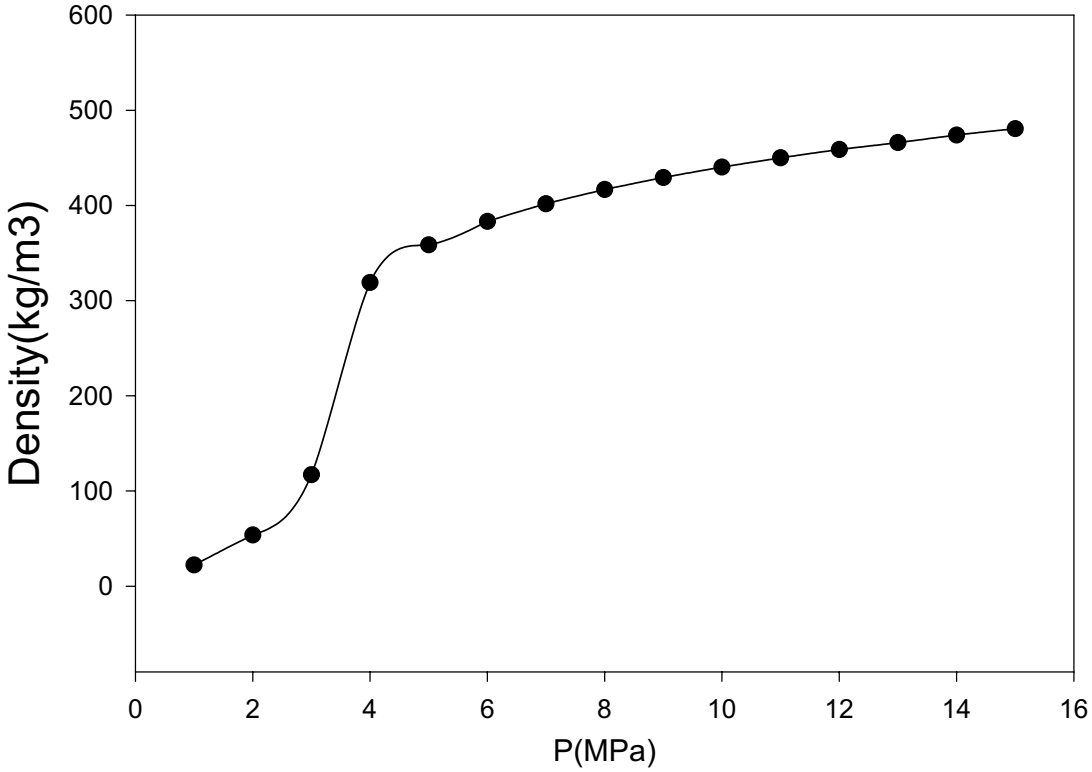

Figure 3. Density vs. pressure mixture of 55%(V) pentane and 45%(V) hexane.

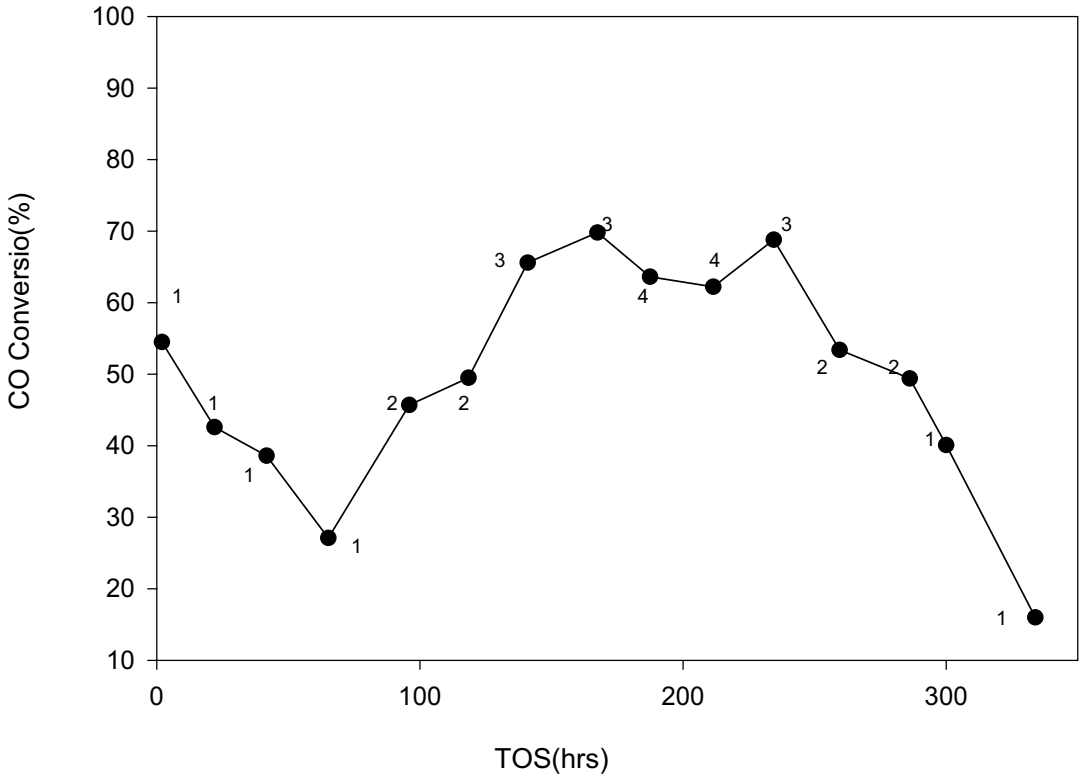

Figure 4. Run YQZ 304. CO conversion vs. TOS (T = 220^{o}C, P_{total} = 8.0 mpa, P_{syngas} = 2.0 mpa, H_2:CO = 2:1; 1 = P_{He} = 6.0, P_{C5+C6} = 0; 2 = P_{He} = 4.0, P_{C5+C6} = 2.0; 3 = P_{He} = 2.5, P_{C5+C6} = 3.5; 4 = P_{He} = 0, P_{C5+C6} = 6.0).

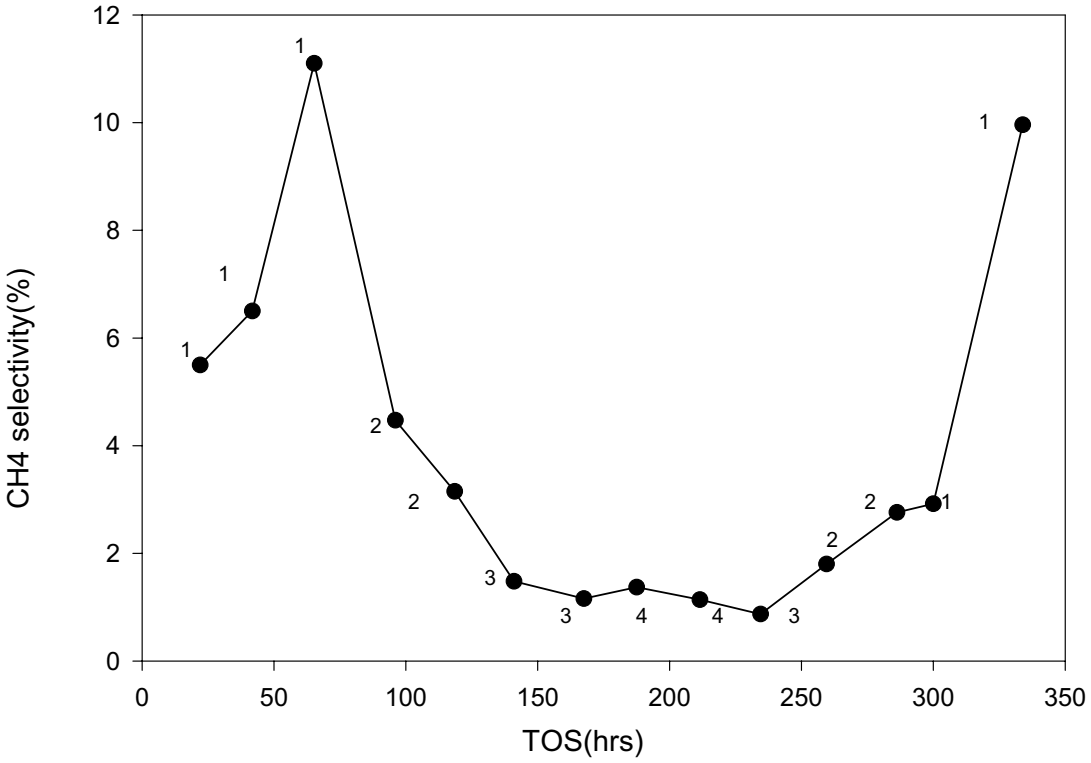

Figure 5. Run YQZ 304. CH_4 selectivity vs. TOS (T = 220^{o}C, P_{total} = 8.0 mpa, P_{syngas} = 2.0 mpa, H_2:CO = 2:1; 1 = P_{He} = 6.0, P_{C5+C6} = 0; 2 = P_{He} = 4.0, P_{C5+C6} = 2.0; 3 = P_{He} = 2.5, P_{C5+C6} = 3.5; 4 = P_{He} = 0, P_{C5+C6} = 6.0).

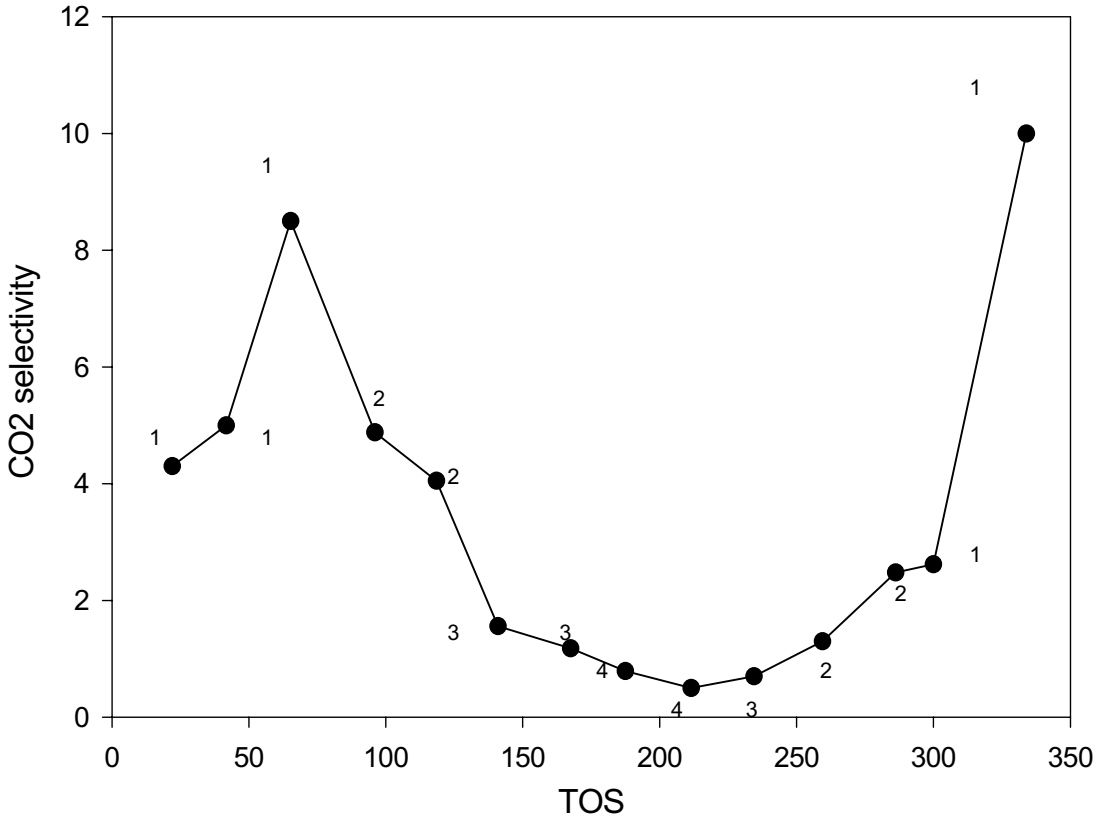

Figure 6. Run YQZ 304. CO_2 selectivity vs. TOS (T = 220^{O}C, P_{total} = 8.0 mpa, P_{syngas} = 2.0 mpa, H_2:CO = 2:1; 1 = P_{He} = 6.0, P_{C5+C6} = 0; 2 = P_{He} = 4.0, P_{C5+C6} = 2.0; 3 = P_{He} = 2.5, P_{C5+C6} = 3.5; 4 = P_{He} = 0, P_{C5+C6} = 6.0).

Task 9. Cobalt Catalyst Life Testing

The objective of this task is to obtain life data on baseline cobalt Fischer-Tropsch catalysts.

No scheduled for further activity to report.

Task 10. Cobalt Catalyst Mechanism Study

The objective of this task is to determine the impact of secondary reactions on the relationship of cobalt Fischer-Tropsch catalysts under conditions appropriate to slurry bubble column reactors.

No scheduled or further activity to report.

Task 11. University of California, Berkeley (Subcontract)

The objective of this task is the characterization of the structure and function of active sites involved in the synthesis of high molecular weight hydrocarbons from CO and H_2 on multi-component catalysts based on Fe as the active component.

Table of Contents

I. FISCHER-TROPSCH SYNTHESIS ON IRON CATALYSTS

1. Background

1.1. Structure and Function of Active Phases in Fischer-Tropsch Synthesis

Fe-based oxides have been used as commercial catalysts for Fischer-Tropsch synthesis (FTS) to produce a large variety of paraffin and olefin products, ranging from methane to high molecular weight waxes [1]. During activation by synthesis gas and subsequent FTS reaction, several phases including metallic iron, iron carbides and iron oxides are known to co-exist at steady-state conditions [2-5]. The distribution and amounts of these phases depend on exposure to various activation and reaction conditions, leading to different catalytic performances in FTS. Some researchers [6] have proposed that surface iron atoms are responsible for FTS activity, while some others considered surface carbides or a mixture of carbides [7,8] and metallic iron [9] to be the active phase. There are also some reports that suggest that magnetite Fe_3O_4 is the active phase in FTS [10-12]. Although these studies have each provided some evidence to support their specific proposals about the active phase, the available information remains phenomenological, and a method to identify the active phase during reaction and to count the number of active sites has not yet been established.

Based on the previous research on Co [13,14] and Fe catalysts [15,16] for FTS as well as our last quarterly work on TPSR of Fe oxides in H_2, our characterization during this research period involved temperature-programmed reactions of Fe-based catalysts with flowing streams of CO or H_2-CO mixtures. We monitored the gas phase concentrations throughout the reduction and carburization processes by means of an on-line mass spectrometer, and followed the evolution of bulk phases and crystal size by X-ray diffraction and of surface area by nitrogen physisorption measurements. In this way, we can determine the temperature required for the formation of Fe carbides as well as the stoichiometry and structure of such carbides. Our goal is to develop a new synthesis method to improve the compositional and structural purity of Fe carbides formed, and consequently to refine the structure-function relationships that we have previously proposed to interpret the catalytic behavior of Fe-based catalysts.

1.2. Effects of Zn, K and Cu

Many components have been added to Fe catalysts in order to improve their mechanical and catalytic properties. Our previous studies have shown that zinc, alkali and copper [16,17] promote the catalytic properties of Fe oxides. Zinc oxide, as a non-reducible oxide in FTS conditions, appears to stabilize the surface area of Fe oxide. Alkali, as a modifier of the adsorption enthalpies of H_2 and CO, increases the selectivity to desired C_{5+} products. Copper promotes the carburization processes and decreases the temperature required for the activation of iron oxide. Here, our efforts have focused on Fe-Zn-K-Cu catalysts. We have prepared a series of Zn and Fe co-precipitated oxides with varied Zn/Fe ratios and then introduced varying amounts of K and Cu. We are examining the surface area, bulk structure, required reduction and carburization temperatures as well as the catalytic behavior of these catalysts, in order to identify optimum Zn/Fe ratios and Cu and K contents that give maximum site density and catalytic activity.

2. Synthesis Procedures for Fe-Zn-K-Cu Oxides

All catalysts were prepared by co-precipitation of zinc and iron nitrates at a constant pH of 7.0 in order to form porous mixed oxides. Then, these oxide precursors were impregnated with an aqueous solution of potassium and copper salts using incipient wetness methods. The Zn/Fe oxide precursors were prepared first. Fe nitrate (1.4 M) and Zn nitrate (3.0 M) solutions were mixed at a given atomic Zn/Fe ratio. A solution of ammonium carbonate (1 M) was prepared separately. Deionized water (ca. 50 ml) was added into a large flask, which was heated on a hot plate with a magnetic stirrer and held at 80 ^{o}C throughout the preparation process. The mixed Zn/Fe solution was added at 2 cm^3/min flow into the flask through a feeding pump. At the same time, the ammonium carbonate solution was fed separately, and its flow was controlled to maintain the slurry pH at 7±0.1, as monitored by a pH meter. The resulting precipitates were washed several times with about 1 *li* water per gram of catalyst, dried at 120 ^{o}C overnight, and then calcined at 350 ^{o}C for 1 h. The calcined material was promoted with 2 at.% K using K_2CO_3 solution (0.16 M) by incipient wetness and then dried. The same process was repeated in order to promote samples with 1 at.% Cu using $Cu(NO_3)_2$ solutions (0.16 M). Finally, the dried material was treated in dry air at 400 ^{o}C for 4 h. This final calcination temperature was chosen from temperature-programmed oxidation data, which showed that this temperature is sufficient to decompose all metal nitrates and carbonates except K_2CO_3. The catalysts contain CuO, ZnO, Fe_2O_3 and K_2CO_3. These catalysts were pressed at 443 MPa into pellets, lightly crushed, and then sieved to retain the 80-140 mesh fraction for FTS reaction.

3. Catalyst Characterization

3.1. Protocols for the Characterization of Fe-based FTS Catalysts

This research program addresses the synthesis and the structural and catalytic characterization of active sites in Fe-based catalysts for FTS. We have designed a matrix of samples that contains a systematic range of multi-components catalysts in order to determine the number and type of surface sites present on fresh catalysts and on samples during and after FTS reaction (Table 1.1). Our objective is to develop rigorous relationships between the synthesis methods, the resulting catalyst structures, and their function in FTS reactions.

3.2. In-Situ X-ray Absorption (XAS) Studies on Fe Catalysts

In-situ X-ray absorption near edge (XANES) and extended X-ray absorption fine structure (EXAFS) analyses provide us with the information about the oxidation states and the local structure of catalysts during FTS. In this reporting period, we continued our X-ray absorption studies at the Stanford Synchrotron Radiation Laboratory (SSRL) with emphasis on Fe K-edge measurements on our standard samples and on a series of fresh and used Fe-Si catalysts provided by Dr. Burtron A. Davis at the Center for Applied Energy Research (CAER) of University of Kentucky (abbreviated as CAER's sample hereafter).

Table 1.1. Matrix of Fe-Zn-K-Cu samples and characterization methods for FTS reaction

<table>
<tr><th colspan="3">Nominal Composition of the Catalysts</th><th rowspan="2">Characterization Before and After FTS</th><th rowspan="2">FTS reaction</th></tr>
<tr><th>Zn/Fe mole ratio</th><th>K/(Fe+Zn) (at.%)</th><th>Cu/(Fe+Zn) (at.%)</th></tr>
<tr><td rowspan="6">0</td><td rowspan="2">0</td><td>0</td><td rowspan="19">XRD

Surface area

In-situ XAS

H_2-TPR

CO-TPR</td><td rowspan="19">Effect of reaction condition

220 ^oC
21.4 atm

235 ^oC
21.4 atm

270 ^oC
5 atm

Effect of CO_2 addition

Isotopic studies</td></tr>
<tr><td>1</td></tr>
<tr><td rowspan="3">2</td><td>0</td></tr>
<tr><td>1</td></tr>
<tr><td>2</td></tr>
<tr><td>4</td><td>1</td></tr>
<tr><td rowspan="3">0.05</td><td>0</td><td>0</td></tr>
<tr><td>2</td><td>1</td></tr>
<tr><td>4</td><td>2</td></tr>
<tr><td rowspan="6">0.1</td><td rowspan="2">0</td><td>0</td></tr>
<tr><td>1</td></tr>
<tr><td rowspan="3">2</td><td>0</td></tr>
<tr><td>1</td></tr>
<tr><td>2</td></tr>
<tr><td>4</td><td>1</td></tr>
<tr><td rowspan="3">0.2</td><td>0</td><td>0</td></tr>
<tr><td>2</td><td>1</td></tr>
<tr><td>4</td><td>2</td></tr>
<tr><td rowspan="6">0.4</td><td rowspan="2">0</td><td>0</td></tr>
<tr><td>1</td></tr>
<tr><td rowspan="3">2</td><td>0</td></tr>
<tr><td>1</td></tr>
<tr><td>2</td></tr>
<tr><td>6</td><td>1</td></tr>
</table>

We used Fe foil as an energy calibration to perform all the measurements in order to obtain more accurate spectra. We prepared $ZnFe_2O_4$ and Fe_xC, which are possible phases of catalysts during FTS, for XAS measurements. $ZnFe_2O_4$ was prepared by co-precipitation of zinc and iron nitrates (Zn/Fe=1/2) with ammonium carbonate (1M) at 80 ^oC at a constant pH of 7.0. Then, the precipitate was calcined in dried air at 400 ^oC for 4 h followed by at 600 ^oC for 24 h. Fe_xC was prepared by temperature-programmed reaction (10 ^oC/min) of precipitated Fe_2O_3 (0.2g) with CO (100 cm^3/min) at temperatures up to 800 ^oC. Fe_xC was passivated by flowing 1 % O_2 in He for 1 h before removing from the synthesis cell. Five samples from the University of Kentucky consisted of unpromoted precipitated Fe oxides (RJO 249) and its samples used for various lengths of time for FTS (RJO282C, D, G and J) at autoclave well mixed reactors. These samples were finely ground, fixed in a plate window, and sealed with Kapton tape. A metal roller was rolled on sealed samples to make them of the same beam path (1mm). Some samples containing high Fe content were diluted to 7~15 wt.% Fe with graphite powder in order to improve the quality of the spectra.

In addition, we measured the XAS spectra of Fe oxides during the reduction and carburization in CO and in synthesis gas. For *in-situ* Fe K-edge spectra, we diluted the samples with graphite powder in order to produce samples with 7 wt.% Fe. The samples were ground with graphite, pressed into pellets, sieved to retain the 45-60 mesh fraction, and loaded into a quartz capillary cell described in the previous quarterly report.

We measured Fe K-edge spectra on beamline IV-3 (30-100 mA at 3.0 GeV). A silicon (111) monochrometer with an unfocussed beam was used to scan the X-ray absorption spectra. To eliminate higher order harmonics X-rays, the monochromator was detuned by 80% from a 20×3 mm beam, which was defined by the slits in the station, and a 15×1.25 mm beam was allowed to pass through the samples. A Fe foil (5μm) was mounted right before the second detector in order to measure a spectrum for the energy calibration of all the samples. X-ray absorption spectra were obtained in transmission mode. Nitrogen gas was passed through the ion chamber detectors for measuring the intensities of incident (I_0) and transmitted (I_1 and I_2) X-rays.

3.3 Fe K-edge XAS Measurement for Standard Samples

3.3.1. Fe K-Edge XANES

The Fe K-edge XAS spectra of Fe_2O_3, Fe_3O_4, FeO, $ZnFe_2O_4$ and Fe_3C are shown in Figure 1.1. The spectra for all the Fe oxides show a strong absorption edge derived from the transition of *1s* electron to the continuum; the feature is referred to as the white line. Fe oxides also show a pre-edge peak below the absorption edge, which is assigned to an allowed dipole transition from a s-state to an unoccupied p-state. The XAS spectrum for Fe_xC shows a shoulder near the edge, but no white line. Figure 1.2 shows the XANES spectra of Fe oxides and Fe_xC compounds with known structure. The pre-edge peaks of Fe oxides reflect a *1s* to *3d* electronic transition, which is dipole-forbidden in centrosymmetric structures, but becomes allowed in tetrahedral or distorted octahedral structures because of p-d orbital mixing. Bulk Fe_2O_3 has a corundum structure where six

oxygen atoms form an octahedron around Fe atoms. However, the distance of Fe-O is not equivalent. Fe has four nearest O neighbors and two close O neighbors, in other words, Fe is located in distorted octahedral holes between O atoms. Therefore, the XAS near edge spectrum of Fe_2O_3 shows a pre-edge peak. Fe_3O_4 has the spinel structure with one-third Fe in tetrahedral holes and two-thirds in octahedral holes. Those Fe atoms in tetrahedral holes exhibit its characteristic pre-edge features. FeO has the rock-salt structure, but it is always deficient in Fe, so it is not in perfect octahedral holes, and thus it shows slight pre-edge feature. $ZnFe_2O_4$ is also of inverse spinel structure in which Fe is surrounded by six oxygen atoms in an octahedron. However, the Fe-O octahedron is easily distorted and some orbital mixing between d-orbital of Fe and p-orbital of oxygen atoms occurs, leading to the presence of pre-edge. The pre-edge peak decreases in the order of Fe_3O_4>Fe_2O_3>$ZnFe_2O_4$>FeO. Fe_xC has an absorption peak around the pre-edge region of Fe oxides, but shows no pre-edge feature.

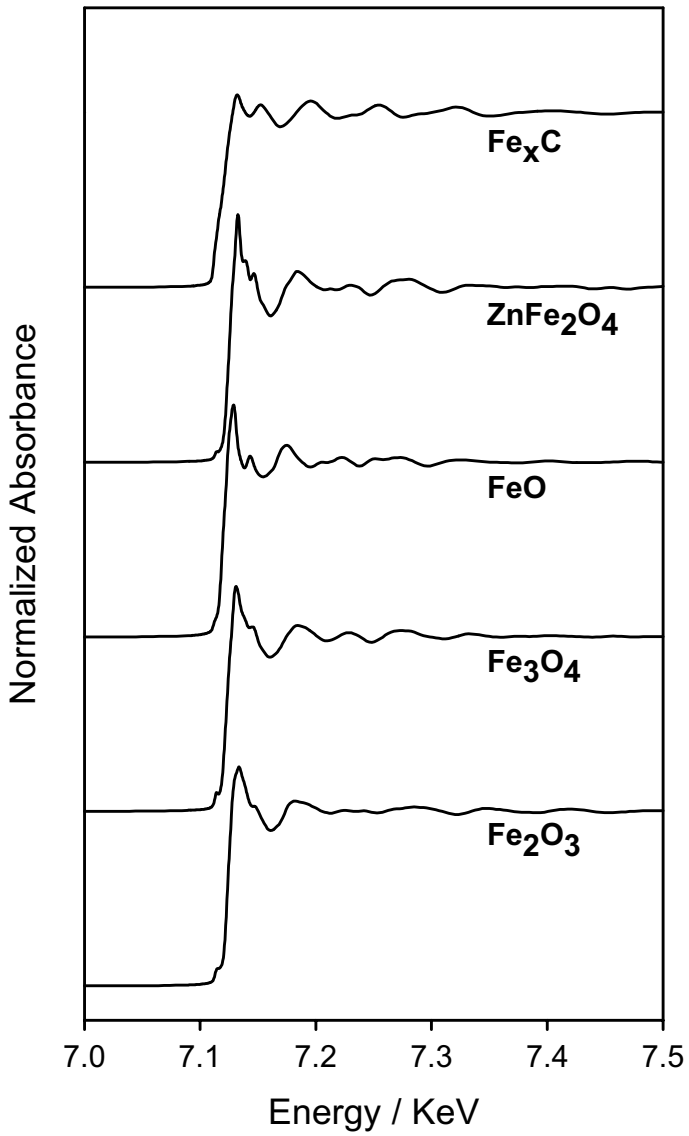

Figure 1.1. Fe K-edge XAS spectra of Fe standard compounds: Fe_2O_3, Fe_3O_4, FeO, $ZnFe_2O_4$ and Fe_xC. (Spectra measured at ambient temperature and atmospheric pressure)

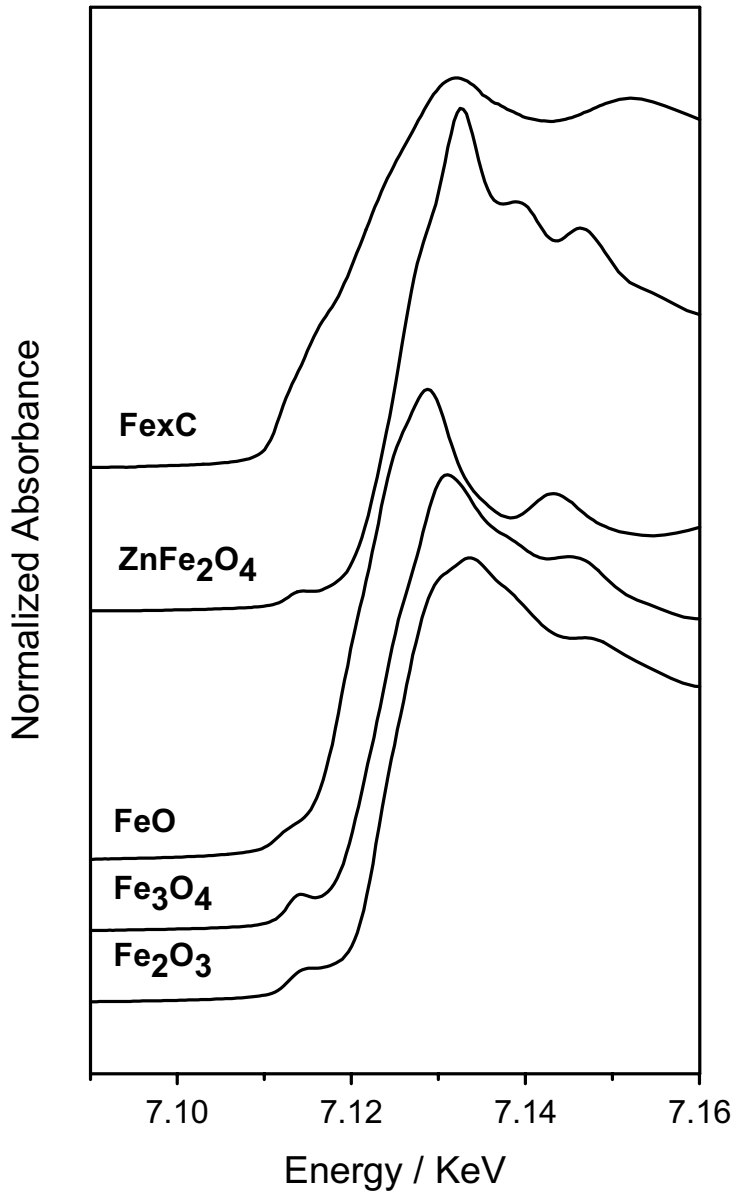

Figure 1.2. Fe K-edge XANES spectra of Fe standard compounds: Fe_2O_3, Fe_3O_4, FeO, $ZnFe_2O_4$ and Fe_xC. (Spectra measured at ambient temperature and atmospheric pressure)

3.3.2 Fe K-Edge XANES Derivatice Spectra

Figure 1.3 shows the Fe K-edge XANES derivative spectra for standard compounds Fe_2O_3, Fe_3O_4, FeO, $ZnFe_2O_4$, and Fe_xC. All the Fe oxides show a pre-edge energy at 7.113 KeV with FeO showing a slight shift of the pre-edge to lower energies. Fe_2O_3, Fe_3O_4, and FeO show Fe K-edge energies at 7.123, 7.124 and 7.119 KeV, respectively, whereas $ZnFe_2O_4$ shows the first inflection point at 7.126 KeV. Fe_xC gives a K-edge

energy at 7.112 KeV, which is the same as that of metallic Fe. We use the first inflection point beyond the pre-edge as the absorption threshold energy.

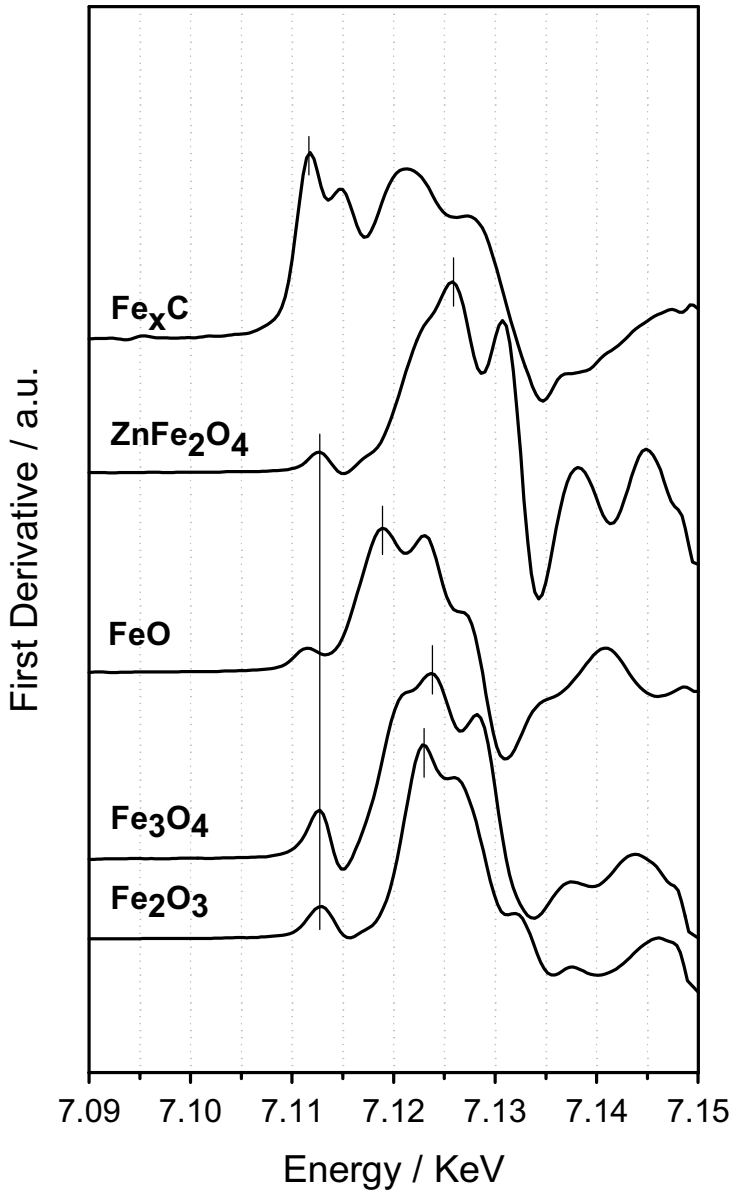

Figure 1.3. Fe K-edge XANES derivative spectra of Fe standard compounds: Fe_2O_3, Fe_3O_4, FeO, $ZnFe_2O_4$ and Fe_xC. (Spectra measured at ambient temperature and atmospheric pressure)

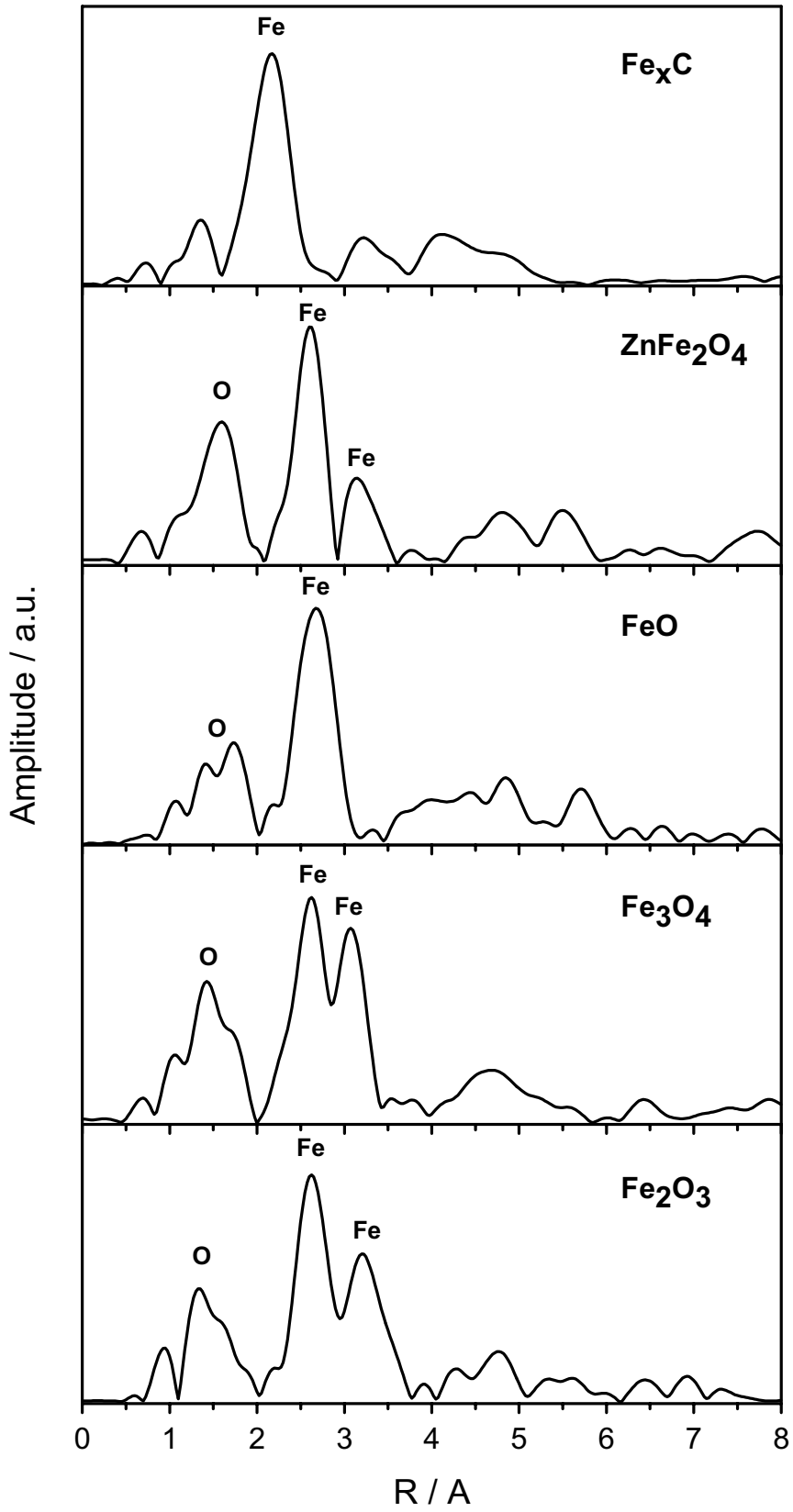

Figure 1.4. EXAFS of Fe K-edge for Fe standard compounds: Fe_2O_3, Fe_3O_4, FeO, $ZnFe_2O_4$ and Fe_xC. (Spectra measured at ambient temperature and atmospheric pressure)

3.3.3. Fe K-Edge EXAFS

Figure 1.4 shows the Fe K-edge Fourier transforms of the extended X-ray absorption fine structure (EXAFS) of standard compounds Fe_2O_3, Fe_3O_4, FeO, $ZnFe_2O_4$ and Fe_xC. k^3-weighting, which compensates for the reduction of the EXAFS oscillation in the high k-region and diminishes the effect of the edge jump and the ambiguity of E_o, is used for the analysis of EXAFS in order to emphasize the contribution of heavier atoms. For Fe_2O_3, Fe_3O_4, and $ZnFe_2O_4$, Fe is coordinated to first nearest neighbor Fe atoms at 2.6 Å and to second nearest neighbor Fe atoms at 3.2 Å for Fe_2O_3 and $ZnFe_2O_4$ and 3.1 Å for Fe_3O_4, respectively; Fe in FeO is coordinated to the first closest neighbor Fe atoms at 2.7 Å. For Fe_xC, its Fourier transform shows a Fe-Fe distance at 2.2 Å, which is the same as that of first nearest Fe neighbor atoms in Fe metal.

3.4. Fe K-edge XAS Measurement for Fe-Zn-K-Cu Oxides

3.4.1. Fe K-Edge EXAFS

In order to study the effect of the incorporation of Zn, K and Cu on the structure of Fe oxides, we also measured the Fe K-edge XAS spectra of coprecipitated Fe-Zn oxides impregnated with K and Cu. Figure 1.5 shows the Fe K-edge EXAFS Fourier transform spectra of Fe-Zn-K-Cu oxides. The EXAFS spectra of Fe-K-Cu oxide and Fe-Zn-K-Cu oxide resemble that of Fe_2O_3, except that the coordination environment of Fe by O atoms is slightly different from that of Fe_2O_3. This indicates that the crystal structure of Fe_2O_3 is mostly retained with the impregnation of K and Cu.

3.5. In-situ Fe K-edge XAS Measurement for Fe Oxides in CO and Synthesis Gas

3.5.1. Fe K-Edge EXAFS

Figure 1.6 shows the Fe K-edge EXAFS Fourier transform spectra of Fe oxides in CO (A) or in synthesis gas (C). The EXAFS spectra (A) of Fe oxide after treatment in CO at temperatures up to 700 ^oC resemble that of standard Fe_xC, indicating that FexC is formed in CO at this temperature. This observation confirmed our conclusion in the previous report that oxygen in Fe-Zn-K-Cu oxide can be removed completely at 500 ^oC in more than 4 h or higher temperature in shorter time. The Fe K-edge EXAFS spectra of Fe oxide in synthesis gas at 250 ^oC for 9 h is more complicated than in CO at 500 ^oC. Fe is mainly coordinated to oxygen atoms, and the spectra resemble that of Fe_3O_4. Also, there is small peak of Fe_xC present in the spectra. This indicates that Fe_2O_3 has been reduced and carburized to a mixture of Fe_3O_4 and Fe_xC under the reaction condition investigated.

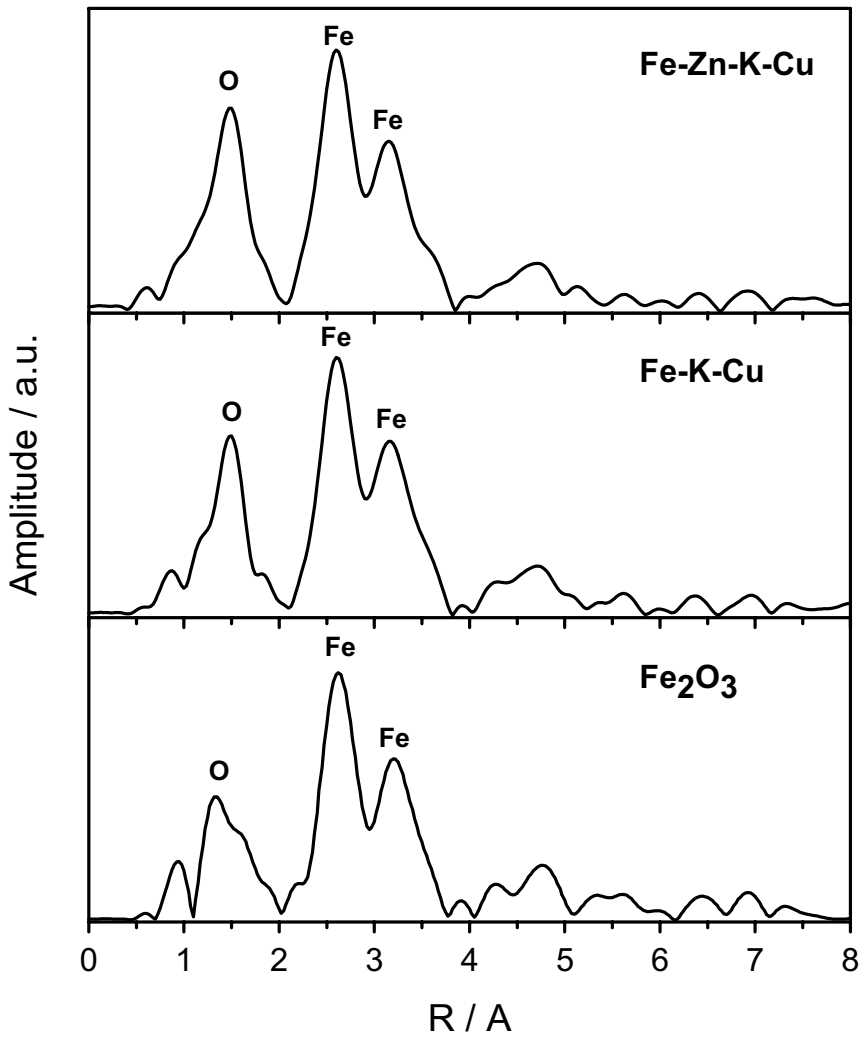

Figure 1.5. Fe-K-edge EXAFS for Fe-Zn-K-Cu oxides. (Zn/Fe=0.1, K/M=0.02, Cu/M=0.01, M=(Fe+Zn))

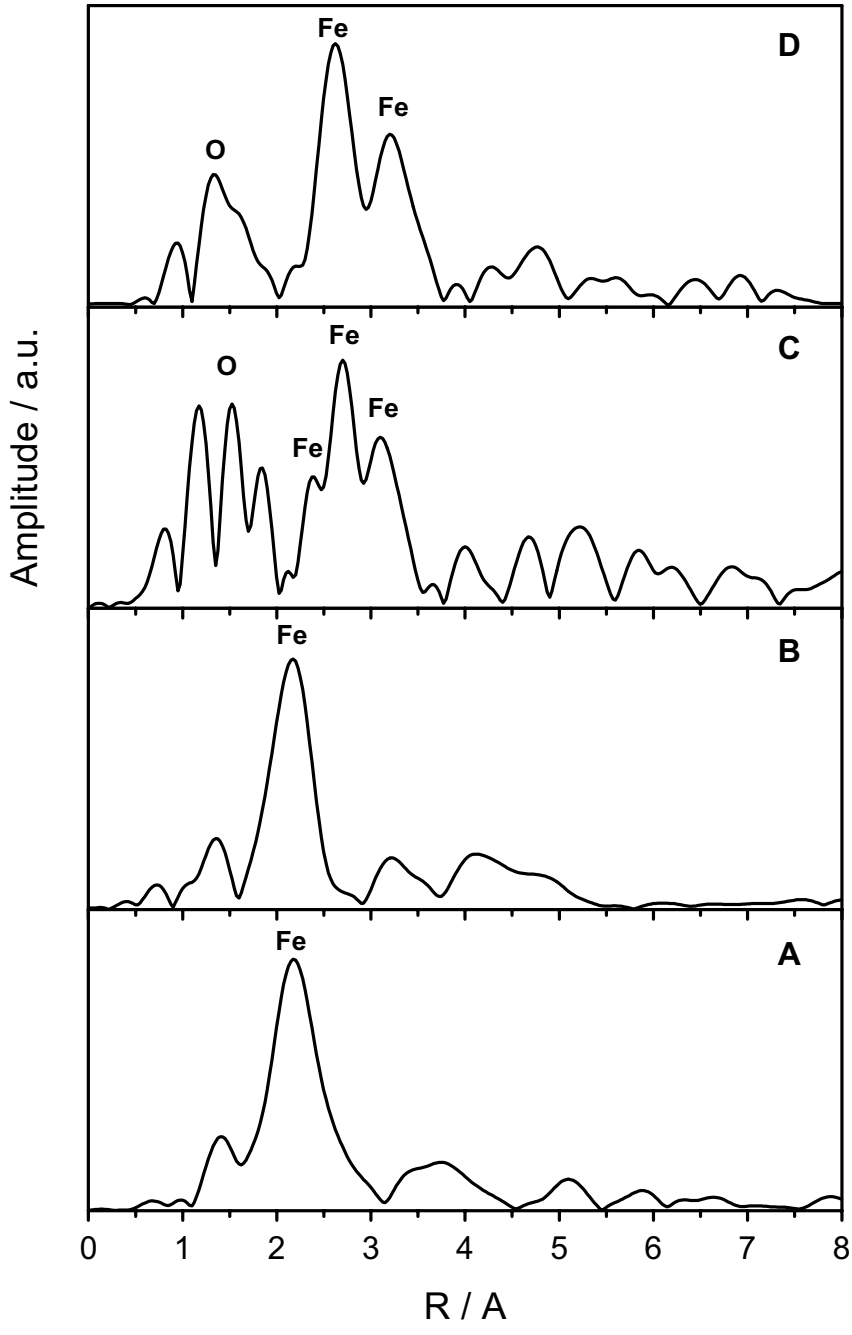

Figure 1.6. *In-situ* Fe K-edge EXAFS Fourier transform spectra. A: Fe oxide in CO at temperatures up to 700 ^{o}C (8 mg sample; 7 wt% Fe; 1.5 cm^3/min), B: Fe_xC; C: Fe oxide in CO/H_2 at 250 ^{o}C for 9 h (8 mg sample; 7 wt% Fe; CO/H_2=1/2, 1.5 cm^3/min); D: Fe_2O_3.

3.6 Fe K-edge XAS Measurement for CAER's Samples

3.6.1 Fe K-Edge XANES

Table 1.2 shows the specification of CAER's samples. RJO249 is unpromoted precipitated Fe oxide and RJO282C, D, G and J are RJO249 used for various lengths of time for FTS at autoclave well mixed reactors. The Mossbauer data provided by CAER shows that the extent of carburization increases and reaches a highest value and then decreases gradually with time on stream. After 432 h, all the carbides were converted to Fe_3O_4.

Figure 1.7 shows the normalized X-ray absorption spectra of RJO249, RJO282C, D, G and J. The smoothness of the spectra indicates that the distortion caused by imperfect monochromatization or improper sample preparation was mostly eliminated. Figure 1.8 shows the X-ray near edge structure (XANES) regions of theses samples. All the spectra present pre-edge peaks and white lines with RJO249 and RJO282G and RJO282J showing prominent features than other two samples. This indicates that more oxide species are present in samples RJO 24, RJO282G and RJO282J.

Table 1.2 Specification of CAER's samples (University of Kentucky)

Sample	RJO249	RJO282C	RJO282D	RJO282G	RJO282J
Reaction time (h)	0	71	121	264	432
Mossbauer Identification	-	70% Fe_5C_2 30% Fe_3O_4	55% Fe_5C_2 45% Fe_3O_4	25% Fe_5C_2 75% Fe_3O_4	Fe_3O_4

3.6.2 Fe K-Edge XANES Derivative Spectra

The XANES derivative spectra are shown in Figure 1.9. All the spectra show a pre-edge energy at 7.113 KeV. The energies at the first inflection point of RJO249, RJO282C, D, G and J are 7.123, 7.124, 7.124, 7.124, 7.125 KeV respectively. Compared with the threshold energy of standard compounds Fe_2O_3, Fe_3O_4, FeO and Fe_xC, which are 7.123, 7.124, 7.119, and 7.112 KeV, it is confirmed that all these samples contain significant amounts of Fe oxides. The increased pre-edge peaks of RJO282C and RJO 282D samples at 7.113 KeV suggest that this sample also contain other species, probably Fe carbides with absorption energy at 7.112 KeV.

3.6.3 Fe K-Edge EXAFS

Figure 1.10 shows the Fe K-edge EXAFS Fourier transforms of each CAER's samples. RJO249 is poorly resolved, indicating the poorly coordinated environment around the absorber. The EXAFS spectra of RJO282C and RJO282D are not well resolved either, indicating the coexistence of difference species. For RJO282C, besides the characteristic

Fe-Fe coordination of Fe_3O_4 at 3.1 Å, it shows a higher peak at 2.2 Å, which coincides with that of Fe_xC. This suggests that it contains both Fe_xC and Fe_3O_4. RJO282D contains less Fe carbide features than that of RJO282C. RJO282G shows mostly similar EXAFS features as that of Fe_3O_4, and RJO282J exhibits the same EXAFS features as that of Fe_3O_4.

3.6.4 Fe K-Edge LC XANES FIT

Table 1.3 shows the linear combination X-ray near edge spectroscopy (LC XANES) fit results of CAER's samples. Figure 1.11 shows the spectrum of RJO282D and its LC XANES fit. The small fit residual (0.8) indicates that they match very well. The LC XANES fit indicates that RJO282C, D and G contain Fe carbides and Fe_3O_4, and RJO 282J contains Fe_3O_4 alone. Although the absolute values of the contents of Fe carbide and Fe_3O_4 in the samples obtained from LC XANES are slightly different from those of Mossbauer spectrascopic measurement, their values show a consistent trend that the extent of carburization increases and reaches a highest value and then decreases gradually with time on stream. After 432 h, all the Fe carbides were converted to Fe_3O_4.

Table 1.3 Fe K-edge LC XANES fit of CAER's samples

Sample	RJO249	RJO282C	RJO282D	RJO282G	RJO282J
LC XANES Fit	-	52% FexC 48% Fe_3O_4	35% FexC 65% Fe_3O_4	2% FexC 98% Fe_3O_4	Fe_3O_4
Fit Residual	-	0.5	0.5	0.8	0.8

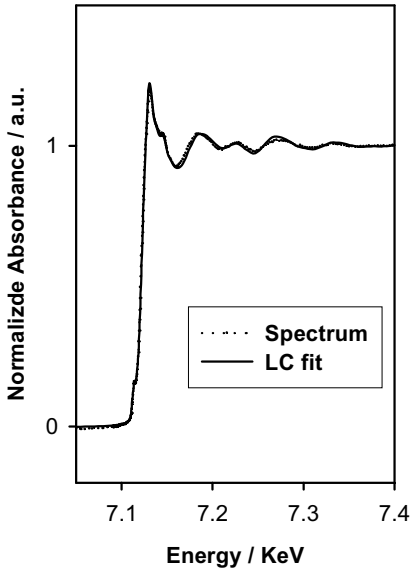

Figure 1.11. LC XANES fit of RJO282D

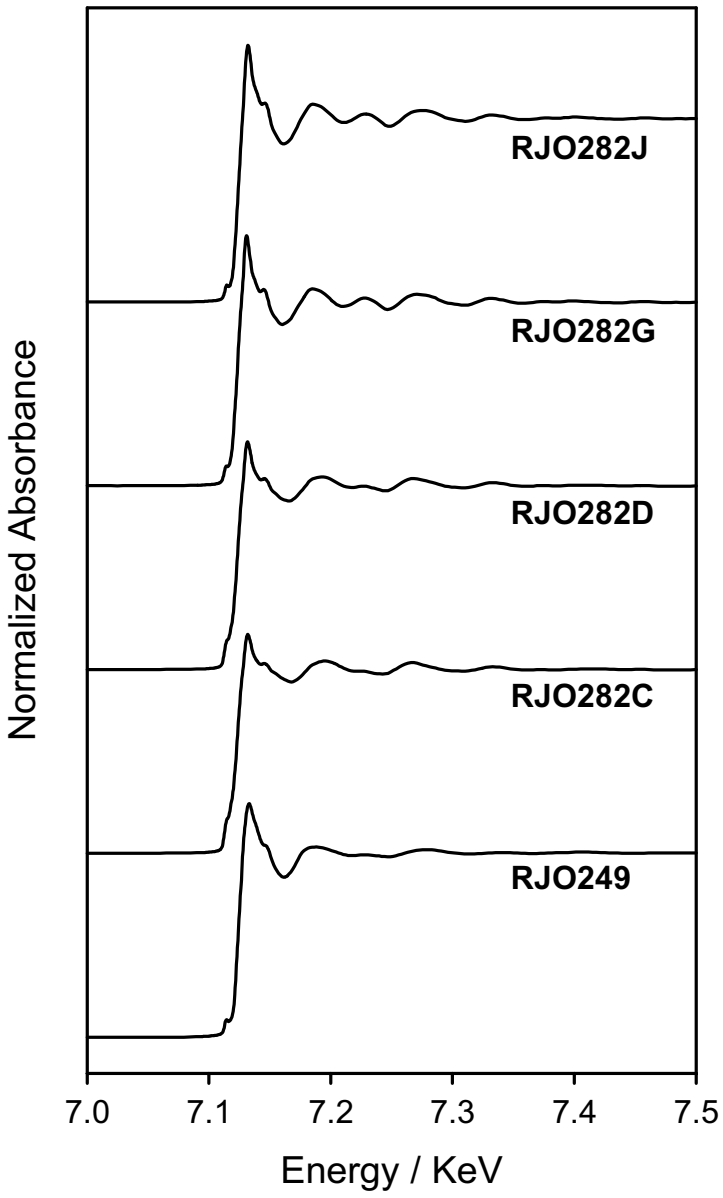

Figure 1.7 Fe K-edge XAS spectra of RJO249, RJO282C, D, G, J.
(Spectra measured at ambient temperature and atmospheric pressure)

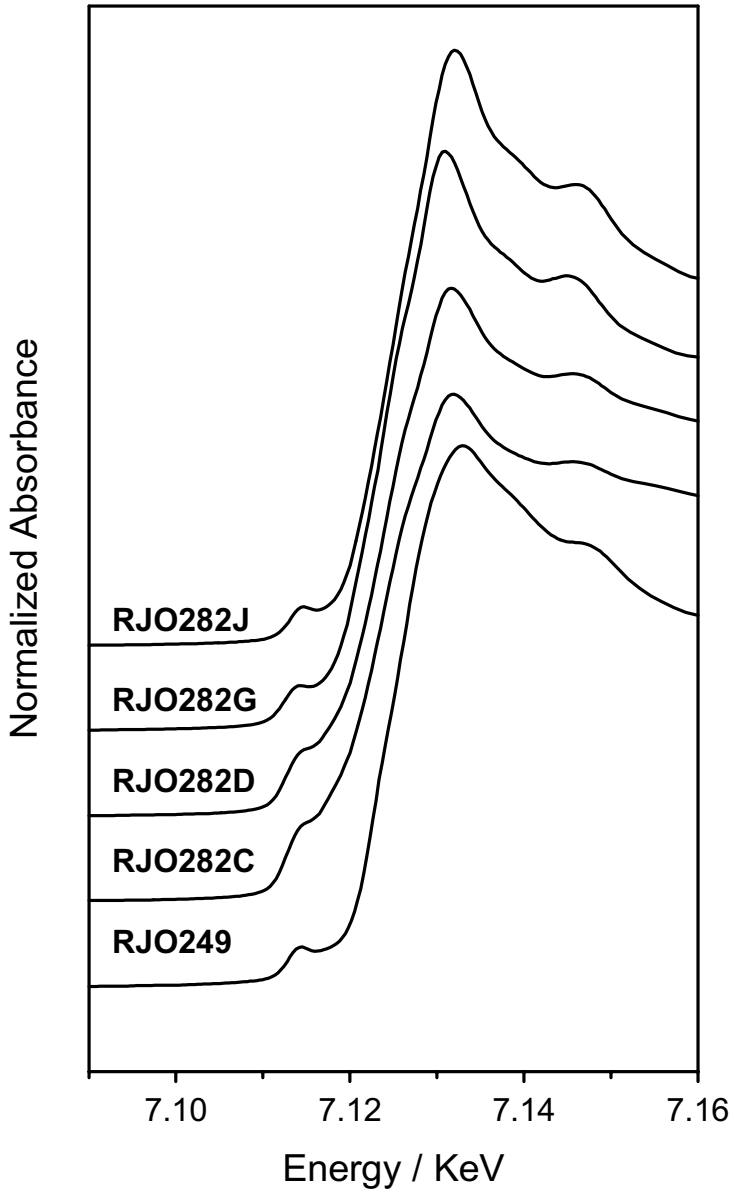

Figure 1.8

Figure 1.8 Normalized Fe K-edge XANES spectra of RJO249, RJO282C, D, G, J. (Spectra measured at ambient temperature and atmospheric pressure)

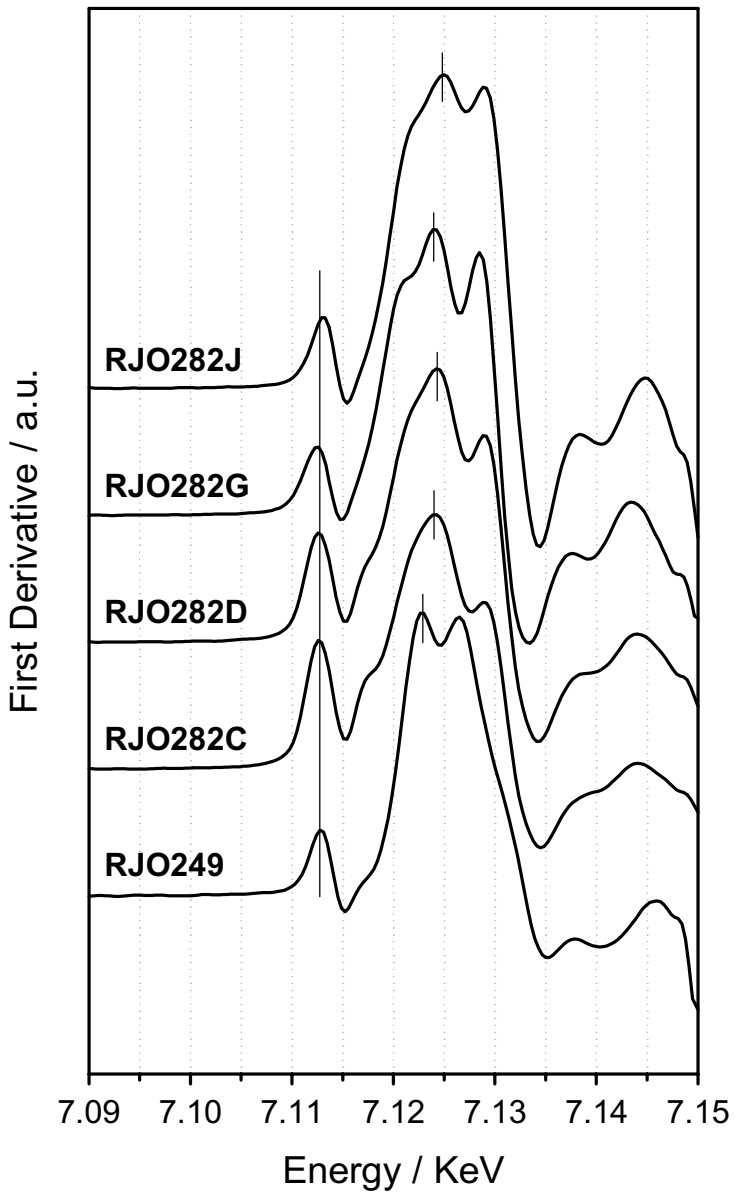

Figure 1.7 Fe K-edge XANES derivative spectra of RJO249, RJO282C, D, G, J. (Spectra measured at ambient temperature and atmospheric pressure)

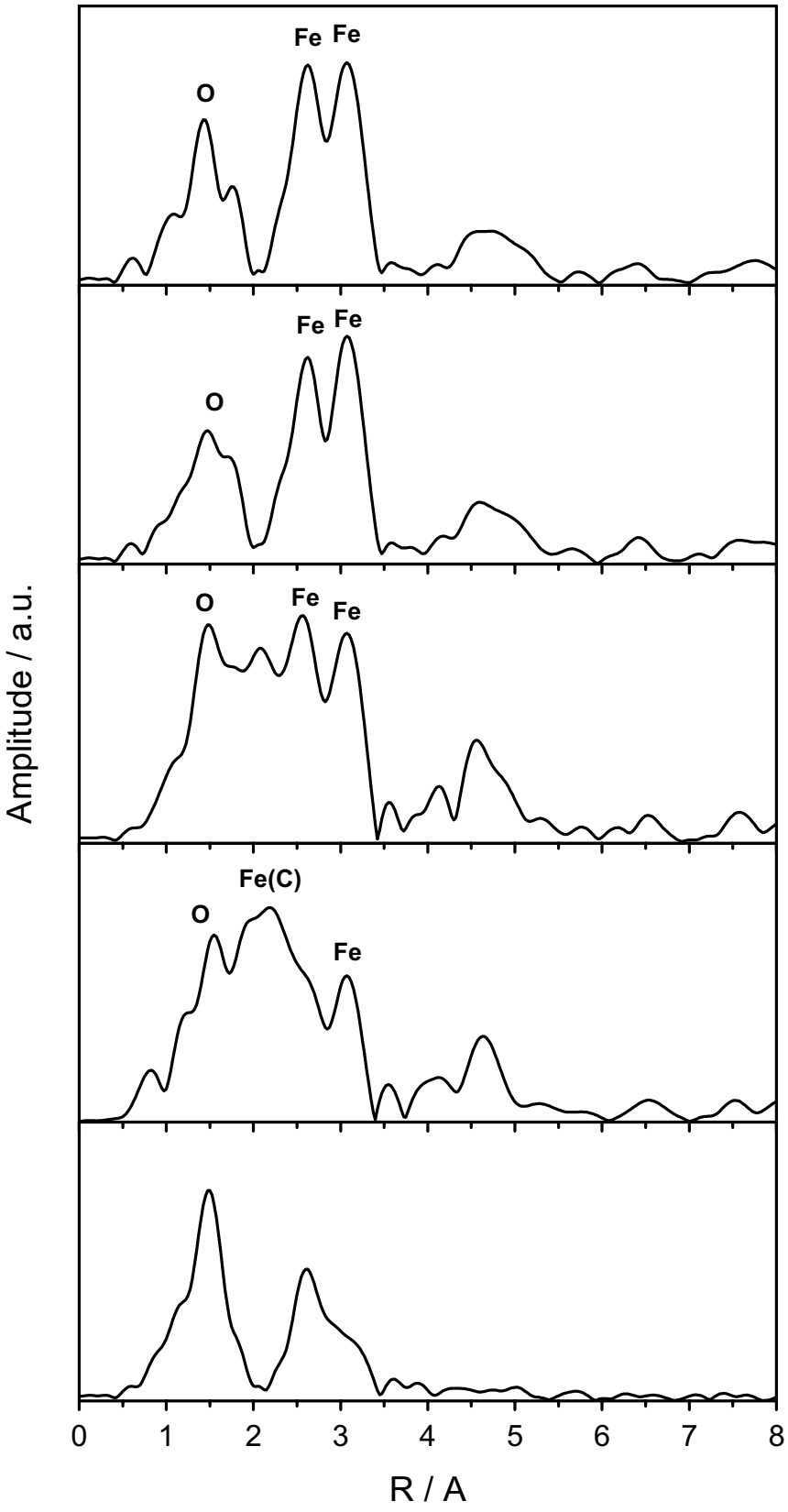

Figure 1.10 Fourier transforms of Fe K-edge EXAFS of RJO249, RJO282C, D, G, J. (Spectra measured at ambient temperature and atmospheric pressure)

4. Fischer-Tropsch synthesis on Fe-based catalysts

4.1. Investigation of H_2/D_2 Isotope Effects on FTS Reactions

During this reporting period, H_2/D_2 kinetic isotope effects (KIE) were investigated on FTS reactions over the Fe-based catalyst (Zn/Fe=0.1, K/M=0.02, Cu/M=0.01) at various space velocities in a fixed-bed reactor at 235 ^oC and 21.4 atm using synthesis gas with a H_2/CO or D_2/CO ratio of 2:1.

4.1.1 H_2/D_2 Effects of FTS Reaction Rates

Figs. 1.12-1.14 show CO conversion rates and hydrocarbon and CO_2 formation rates as a function of CO conversion on the catalyst (Zn/Fe=0.1, K/M=0.02, Cu/M=0.01) at 235 ^oC and 21.4 atm. CO conversion and hydrocarbon formation rates were much higher with D_2/CO than with H_2/CO mixture. In contrast, CO_2 formation rate was lower with D_2/CO than with H_2/CO. It has been proposed that the formation of higher molecular weight hydrocarbons on Fe-based catalyst during FTS reactions is initiated by the addition of a methyl group to a methylene group and that further chain growth occurs by the reaction of methylene group with adsorbed alkyl groups. The alkyl groups then react to form olefins and paraffins via either hydrogen elimination or addition. Consistent with these views of CO hydrogenation, one would expect to observe a normal isotopic effect if D_2 were used instead of H_2.

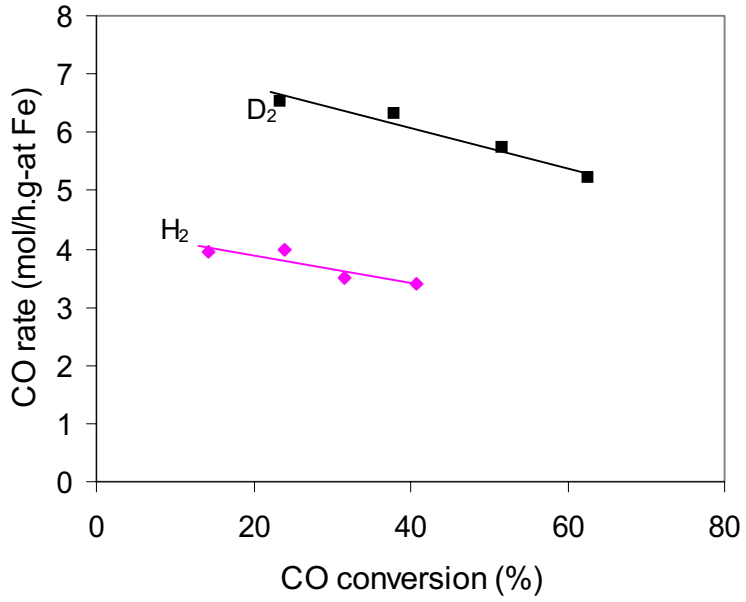

Fig.1.12 CO conversion rate as a function of CO conversion for H_2/CO or D_2/CO reactants (Zn/Fe=0.1, K/M=0.02, Cu/M=0.01) at 235 ^oC and 21.4 atm.

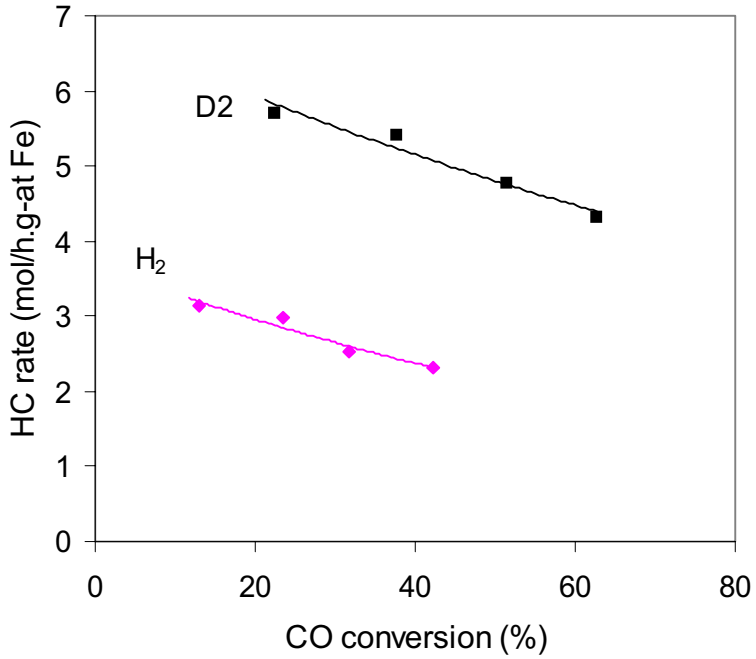

Fig.1.13 Hydrocarbon formation rate as a function of CO conversion for H_2/CO or D_2/CO reactants (Zn/Fe=0.1, K/M=0.02, Cu/M=0.01) at 235 ^oC and 21.4 atm.

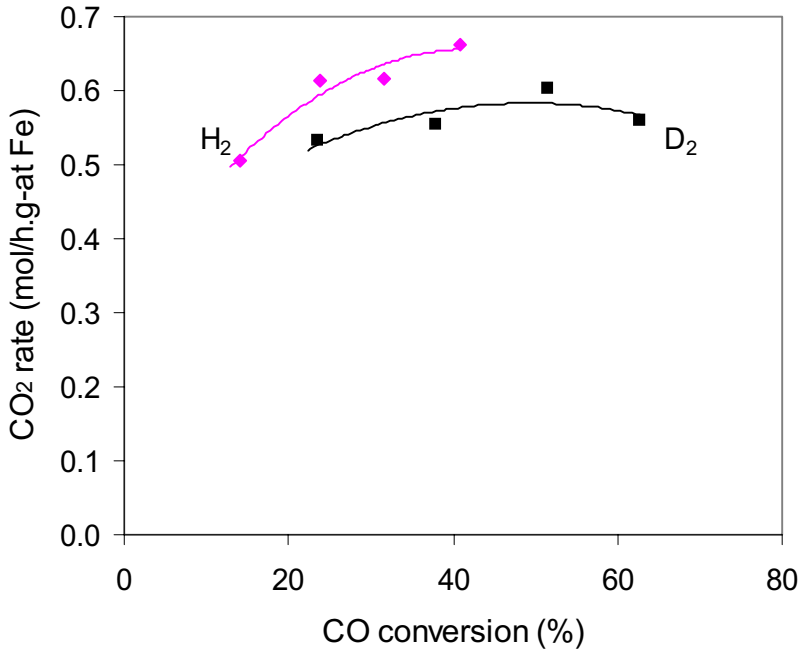

Fig.1.14 CO_2 conversion rate as a function of CO conversion for H_2/CO or D_2/CO reactants (Zn/Fe=0.1, K/M=0.02, Cu/M=0.01) at 235 ^oC and 21.4 atm.

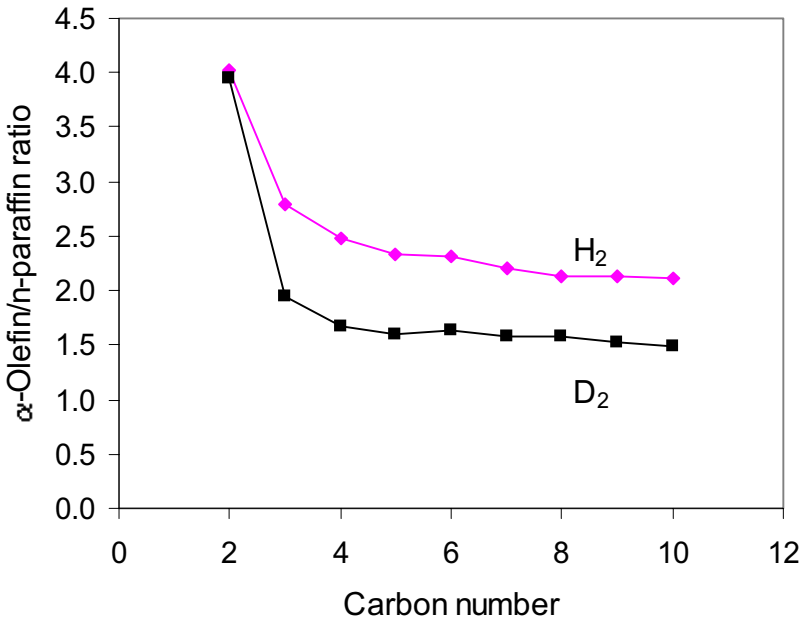

Fig.1.15 α-Olefin/n-paraffin ratio as a function of CO conversion for H_2/CO or D_2/CO reactants (Zn/Fe=0.1, K/M=0.02, Cu/M=0.01) at 235 °C and 21.4 atm.

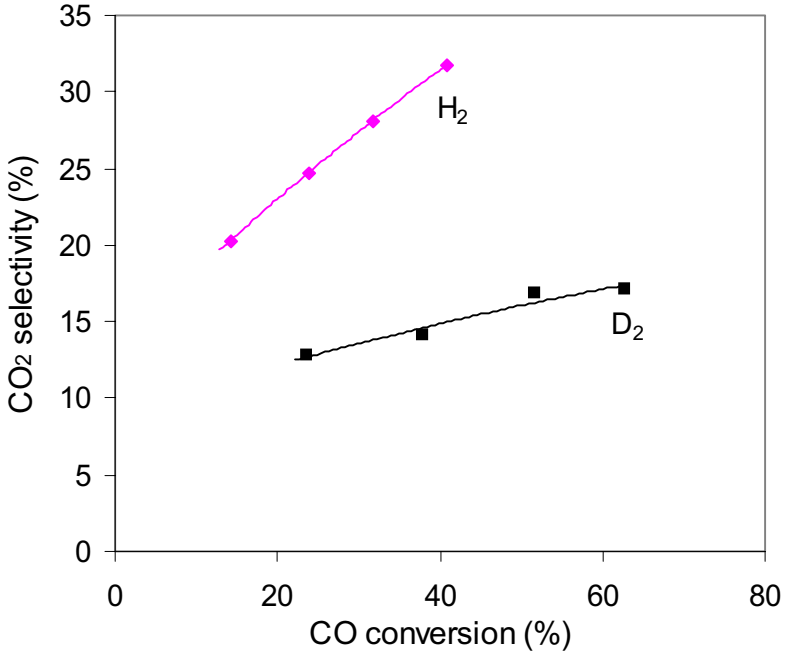

Fig.1.16 CO_2 selectivity as a function of CO conversion for H_2/CO or D_2/CO reactants (Zn/Fe=0.1, K/M=0.02, Cu/M=0.01) at 235 °C and 21.4 atm.

However, we observed an inverse isotopic effect as D_2 was used instead of H_2. Wilson [21] noted that the overall isotopic effect for CO hydrogenation could arise from a combination of kinetic and equilibrium isotope effects, the former favoring the reaction

of H_2 and the latter favoring the reaction of D_2. The inverse isotopic effects of our observations suggested a dominant role of the thermodynamic effects. The higher CO conversion and hydrocarbon formation rates may reflect the stronger adsorption of D_2 than that of H_2 on the Fe-based catalyst. Fig. 1.15 shows α-olefin/n-paraffin ratio as a function of carbon number. Fig. 1.16 shows CO_2 selectivity as a function of CO conversion. The increase in surface H_2 or D_2 concentration on the catalyst increases the probability of hydrogen addition of the adsorbed alkyl to form paraffins and decrease the probability of hydrogen elimination of the adsorbed alkyl to form olefins. The increase in surface H_2 or D_2 concentration also decreases the formation of CO_2 via water-gas shift reaction by causing the removal of the oxygen in CO by adsorbed hydrogen rather than adsorbed CO. Hence, both lower α-olefin/n-paraffin ratio with D_2 as shown in Fig. 1.15 and lower CO_2 selectivity with D_2 as shown in Fig. 1.16 suggest that higher surface concentrations of H isotopes are present when D_2 is used. The higher surface D_2 concentration is due to its larger adsorption equilibrium coefficient. This result is in agreement with previous studies. Soller [22] observed about 1.4 times more adsorption of D_2 than H_2 on Cu powder at 125 ^oC. Larger adsorption coefficients were obtained for D_2 than for H_2 on Ni during the hydrogenation of acetylene [23] and of CO_2 [24].

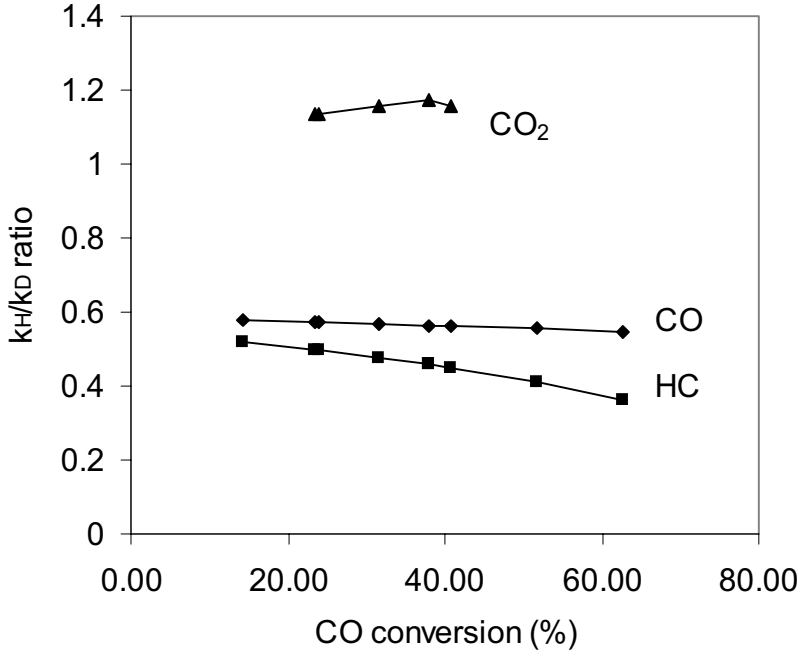

Fig.1.17 k_H/k_D ratio for CO conversion, hydrocarbon and CO_2 formation as a function of CO conversion for H_2/CO or D_2/CO reactants (Zn/Fe=0.1, K/M=0.02, Cu/M=0.01) at 235 ^oC and 21.4 atm.

A reaction rate expression proposed [25] for FTS is

$$-r_{CO+H_2} = \frac{kP_{CO}P_{H_2}^2}{P_{CO}P_{H_2} + bP_{H_2O}}$$

Where b is adsorption parameter and k is rate constant. Based on this rate expression, hydrocarbon formation rate ($-r_{CO+H_2}$) almost linearly increase with hydrogen pressure at low conversion. Since FTS reactions proceed on the surface of the catalyst and surface hydrogen concentration is determined by hydrogen pressure, higher surface hydrogen concentration gave higher hydrocarbon formation rate. Therefore, CO conversion and hydrocarbon formation rates were higher with D_2 at same CO conversion, as shown in Figs. 1.12 and 1.13. Likely, a lower CO_2 formation rate as shown in Fig. 1.14 was also due to the higher surface deuterium concentration since hydrogen is one of products of water-gas shift reaction.

4.1.2 k_H/k_D Ratio

The isotopic effect can be expressed by a ratio of k_H/k_D. k_H and k_D are rate constants for H_2 and D_2, respectively. Since we did not have experimental value for both k_H and k_D at the same CO conversion, we got k_H values by fitting the curve of rate vs. CO conversion for experimental values of k_D and also get a fitted value of k_D for each experimental value of k_H by a similar way.

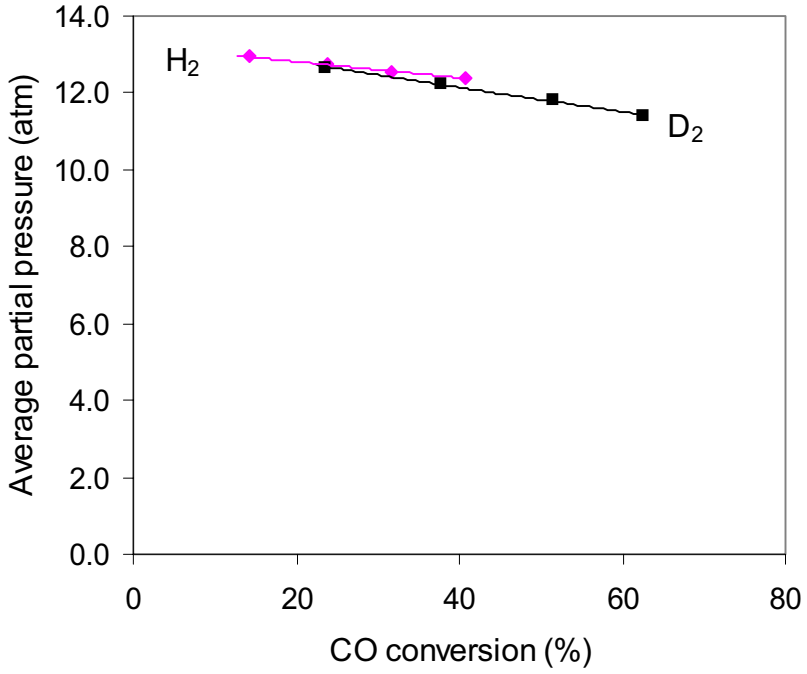

Fig.1.18 Average partial pressure of hydrogen as a function of CO conversion for H_2/CO or D_2/CO reactants (Zn/Fe=0.1, K/M=0.02, Cu/M=0.01) at 235 ^oC and 21.4 atm.

Fig. 1.17 shows k_H/k_D ratio for CO conversion, hydrocarbon and CO_2 formation as a function of CO conversion. The k_H/k_D ratio for hydrocarbon formation was about 0.5 and slightly decrease with increasing CO conversion. The k_H/k_D ratio for CO_2 formation was greater than 1. The inverse isotopic effect for hydrocarbon formation (k_H/k_D <1) and the normal isotopic effect for CO_2 formation (k_H/k_D > 1) are expected because higher surface hydrogen concentration was present when D_2 was used. It is not clear why the k_H/k_D ratio for hydrocarbon formation decreased with increasing CO conversion. The reason might be that the partial pressure of hydrogen changes with CO conversion. Fig. 1.18 shows the partial pressure of hydrogen as a function of CO conversion. It is seen that the partial pressures for both H_2 and D_2 decreased with increasing CO conversion. We speculate that surface hydrogen concentration is more sensitive to the reduction of pressure in gas phase for H_2 than that for D_2 because the adsorption coefficient of D_2 is higher than that of H_2. Accordingly, hydrocarbon formation rate decreased faster with decreasing partial pressure for H_2 than for D_2. Hence, the k_H/k_D ratio for hydrocarbon formation decreased with increasing CO conversion (Fig. 1.17).

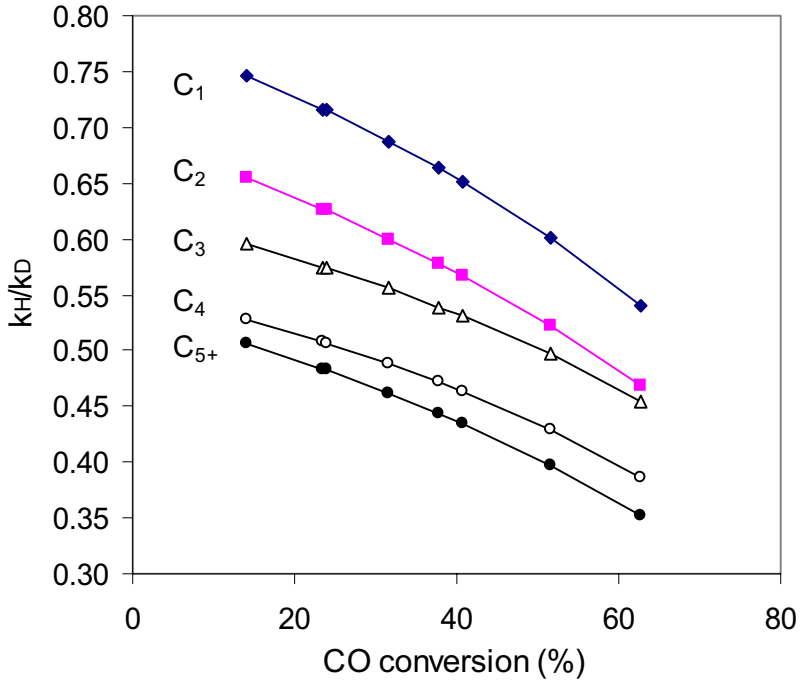

Fig.1.19 k_H/k_D ratios for C_1-C_4 and C_{5+} as a function of CO conversion for H_2/CO or D_2/CO reactants (Zn/Fe=0.1, K/M=0.02, Cu/M=0.01) at 235 ^oC and 21.4 atm.

Fig. 1.19 shows the k_H/k_D ratios of C_1-C_4 and C_{5+} formation as a function of CO conversion. Similarly, all ratios decreased with increasing CO conversion. It is also seen that at the same CO conversion k_H/k_D ratio systematically decreased with carbon number, suggesting that the inverse isotopic effects are more evident for larger hydrocarbons. Deuterium appears to favor the formation of hydrocarbon with higher molecular weight because the selectivity to C_{5+} was higher when D_2 was used (Fig. 1.20). Hence, the k_H/k_D ratio decreased with carbon number.

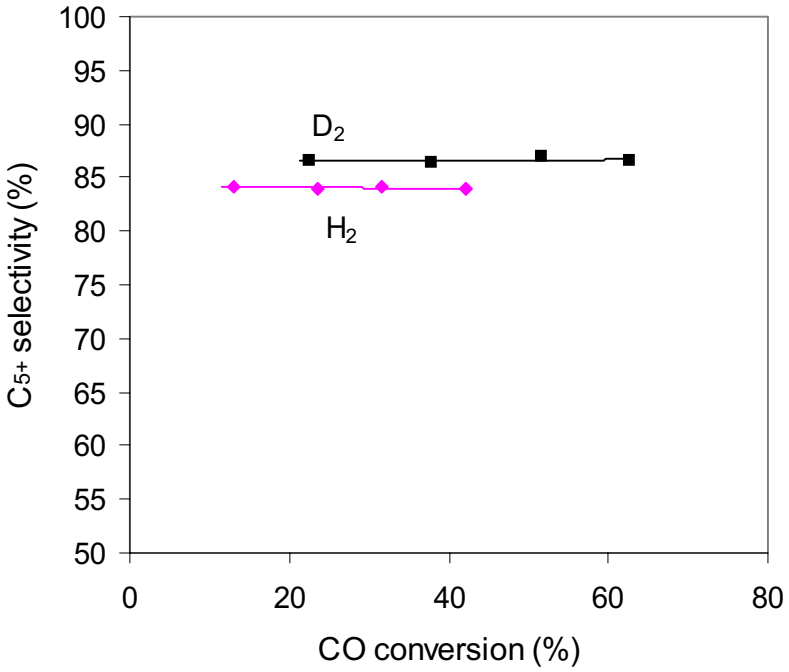

Fig.1.20 C_{5+} selectivity as a function of CO conversion for H_2/CO or D_2/CO reactants (Zn/Fe=0.1, K/M=0.02, Cu/M=0.01) at 235 ^{o}C and 21.4 atm.

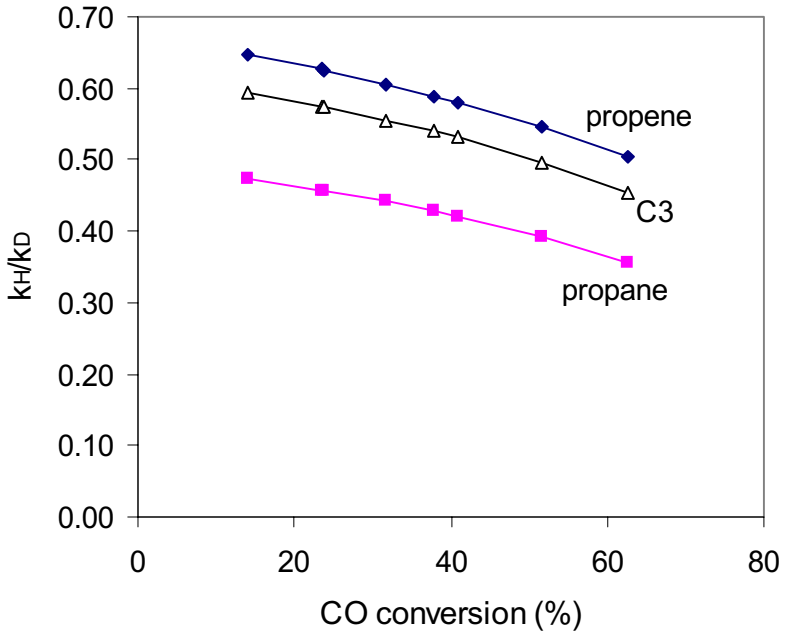

Fig.1.21 The k_H/k_D ratios of propene, propane and total C_3 as a function of CO conversion for H_2/CO or D_2/CO reactants (Zn/Fe=0.1, K/M=0.02, Cu/M=0.01) at 235 ^{o}C and 21.4 atm.

.

The isotopic effect for propene and propane is given in Fig. 1.21. The k_H/k_D ratio for propylene was higher than that for propane. Similar result was obtained for butene and butane (Fig. 1.22), suggesting that the inverse isotopic effect is more evident for paraffins than for olefins. This is because the probability of paraffin formation increased due to higher surface hydrogen concentration when D_2 was used.

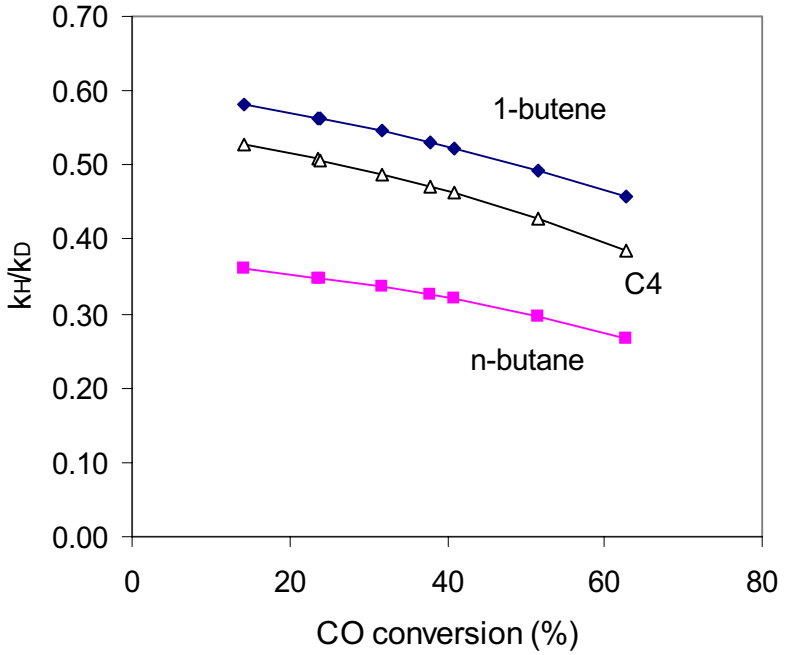

Fig.1.22 The k_H/k_D ratios of 1-butene, n-butane and total C_4 as a function of CO conversion for H_2/CO or D_2/CO reactants (Zn/Fe=0.1, K/M=0.02, Cu/M=0.01) at 235 ^oC and 21.4 atm.

.

II. FISCHER-TROPSCH SYNTHESIS ON COBALT CATALYSTS

1. Background

During last reporting period, D_2O tracer and D_2-H_2 exchange experiments were carried out during FTS. The results showed that the H_2 dissociation was quasi-equilibrated and that water dissociation was largely irreversible during FTS on Co-based catalysts. According to these findings, we proposed water-enhanced propagation in order to explain the enhancement of the synthesis rate by water observed on cobalt catalysts. During this reporting period, an additional reaction pathway was proposed for the Co-catalyzed FTS. We continued the studies of FTS reaction kinetics with focus on the effects of H_2, CO and H_2O partial pressure on FTS rate and selectivity. In addition, we conpleted the data analysis of the previous isotope effect run using H_2 and/or D_2 and obtained the kinetic isotope effects for individual hydrocarbons.

2. Experimental

FTS kinetics was studied using a fixed-bed, single-pass flow reactor. The reactants, H_2 (Matheson, UHP) and CO/N_2 (Matheson, UHP, 81.5/18.5, molar ratio) were introduced into the reactor separately using mass flow controllers (Brooks, model 5850). De-ionized water was added to the reactant feed using a high-pressure syringe pump (Isco, Inc., Model 500D). The cobalt catalyst used was a 21.9 wt% Co/SiO_2 catalyst. The preparation and pretreatment of the cobalt catalyst were described in the previous quarterly report. The reactor was kept at 20 atm, 200°C and $H_2/CO = 2.0$ for the first 100 h in order to allow the catalyst to achieve steady-state operation. The conversion of CO was varied from 5 to 30% by changing the space velocity. N_2 (used as an internal standard), CO, CO_2, and light hydrocarbons (C_1-C_{12}) were analyzed by on-line gas chromatography (Hewlett-Packard 5890) using thermal conductivity and flame ionization detections. Synthesis rate was reported as a site-time yield (molar CO converted per g atom surface Co). H_2/D_2 isotope effects were examined by comparing the rates of FTS using $H_2/CO/N_2$ (62/31/7) and $D_2/CO/N_2$ (62/31/7), which were running at 20 atm, 200°C.

3. FTS on Cobalt-base Catalysts

3.1 H_2/D_2 Isotope Effects

According to the carbide mechanism, FTS proceeds via H_2 dissociation and then stepwise hydrogenation of adsorbed carbon to form methylene monomers. The formation of higher molecular weight hydrocarbons is initiated by the addition of a methylene monomer to a methyl group. Further chain growth occurs by the reaction of methylene monomers with adsorbed alkyl groups. The alkyl groups then react to form olefins and paraffins via either hydrogen elimination or addition [26,27]. Consistent with these views of CO hydrogenation, one would expect to observe an isotopic effect if D_2 is used instead of H_2 in FTS. Such studies with H_2/D_2 may give a better understanding of FTS

reaction mechanism. However, the results available in literature have led to contradictory conclusions [28-31], probably due to a wide variations in operating conditions. In this study, H_2/D_2 isotope effects were examined under realistic FTS conditions favoring high chain growth probability (20 atm, 200°C and $H_2/CO = 2.0$).

The rate of CO consumption is presented in Figure 2.1 as a function of CO conversion. In this study, CO conversion was increased by decreasing space velocity while maintaining all other conditions. Comparing the rate obtained using H_2/CO with that for D_2/CO, we obtained a series of isotope effects (k_H/k_D) for overall CO consumption at several conversions (Figure 2.2). The data presented in Figure 2.1 show that the synthesis rate increased with the increasing CO conversion using either H_2 or D_2. In the previous report, the phenomenon was attributed to the effect of the water produced during FTS. As seen in Figure 2.2, however, the isotope effect (k_H/k_D) for CO consumption is about 0.8, independent of the CO conversion. This value is very close to that reported by Sakharov and Dokukina [28].

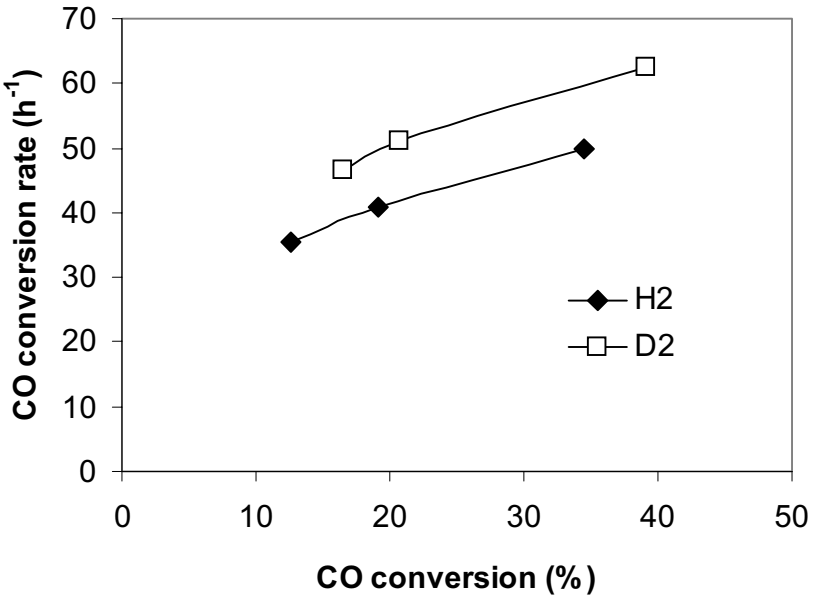

Figure 2.1. Rate of CO consumption versus CO conversion (21.9 wt% Co/SiO_2, 200°C, 20 atm, H_2/CO or $D_2/CO = 2.0$)

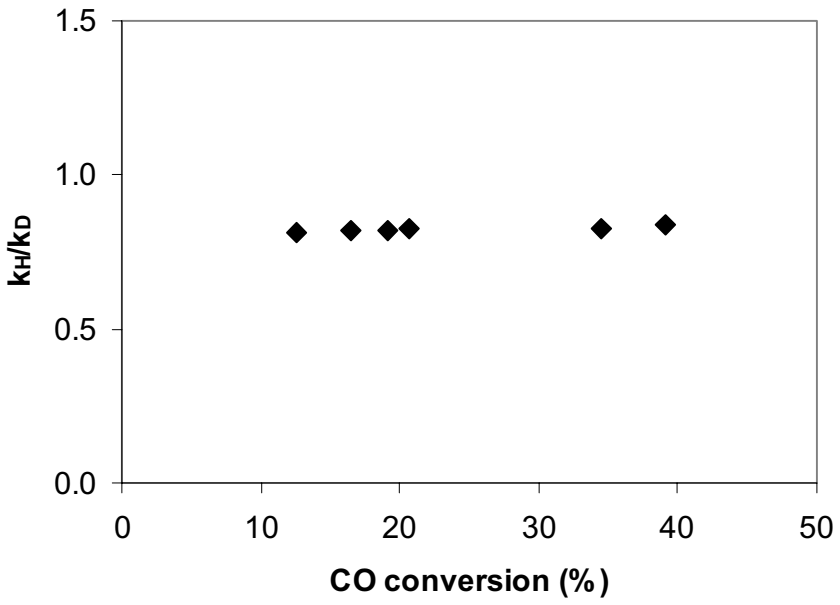

Figure 2.2. Isotope effect for CO consumption versus CO conversion (21.9 wt% Co/SiO_2, 200°C, 20 atm, H_2/CO or D_2/CO = 2.0)

Kinetic isotope effects for each hydrocarbon (C_1-C_7) were also calculated and they are shown in Figures 2.3 to 2.9. Unlike the isotope effect for CO consumption, these effects (k_H/k_D) for individual hydrocarbons change with CO conversion. In general, the effects for paraffins increase with increasing CO conversion, whereas the effects for olefins decrease with increasing CO conversion. This is not surprising when we look at the original rate data shown in Figures 2.10 to 2.16. For example, as seen in Figure 2.15, the C_6H_{12} formation rate decreases slightly with increasing CO conversion, compared to a small increase in C_6D_{12} rate. C_6H_{14} and C_6D_{14} formation rates both increase with increasing CO conversion, but the increase of the C_6D_{14} rate is not as pronounced as for the C_6H_{14} rate. These results suggest that C_nH_{2n} olefins are more reactive in secondary hydrogenation than the corresponding deuterated ones. As a result, the isotope effects (k_H/k_D) for the paraffins increased while those for the olefins decreased with increasing CO conversion.

In order to rule out the interference of secondary reactions, the lines shown in Figures 2.3 to 2.9 were extrapolated to zero conversion. Thus, isotope effects (k_H/k_D) for the paraffins (C_2-C_7) were between 0.7 and 0.9 and for methane was about 1.0. Meanwhile, normal isotope effects (around 1.1) were obtained for the olefins (C_2-C_7). Our results are somewhat different from those reported by Kellner and Bell [31]. They reported an inverse isotope effect (k_H/k_D = 0.9) for methane formation and no systematic effect for higher hydrocarbons on a Ru/SiO_2 catalyst (10 atm, < 1.5% conversion).

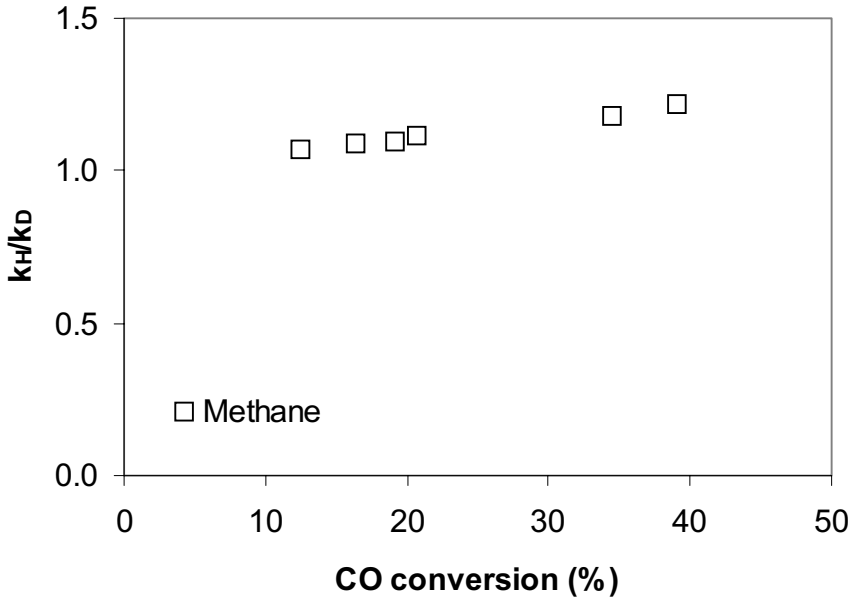

Figure 2.3. Isotope effect for methane versus CO conversion (21.9 wt% Co/SiO_2, 200°C, 20 atm, H_2/CO or D_2/CO = 2.0)

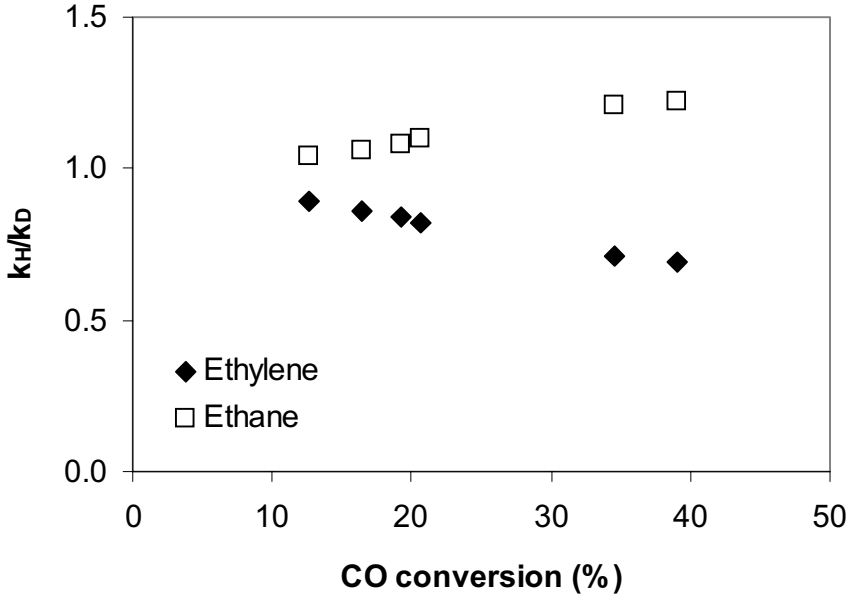

Figure 2.4. Isotope effect for C_2 products versus CO conversion (21.9 wt% Co/SiO_2, 200°C, 20 atm, H_2/CO or D_2/CO = 2.0)

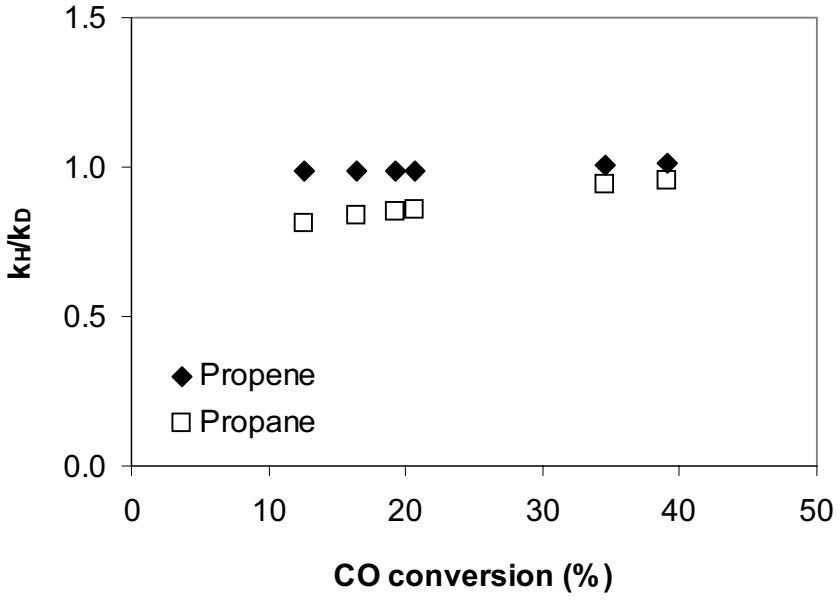

Figure 2.5. Isotope effect for C_3 products versus CO conversion (21.9 wt% Co/SiO_2, 200°C, 20 atm, H_2/CO or D_2/CO = 2.0)

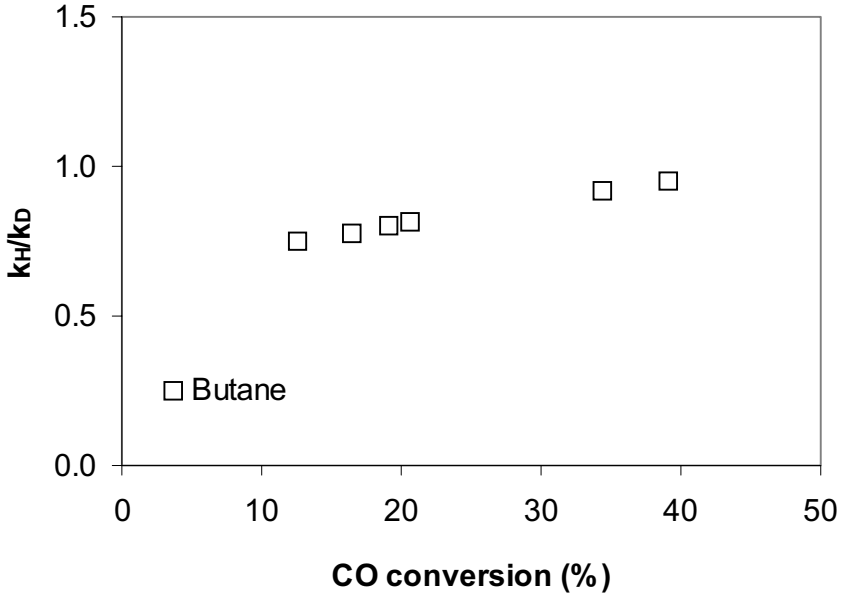

Figure 2.6. Isotope effect for butane versus CO conversion (21.9 wt% Co/SiO_2, 200°C, 20 atm, H_2/CO or D_2/CO = 2.0)

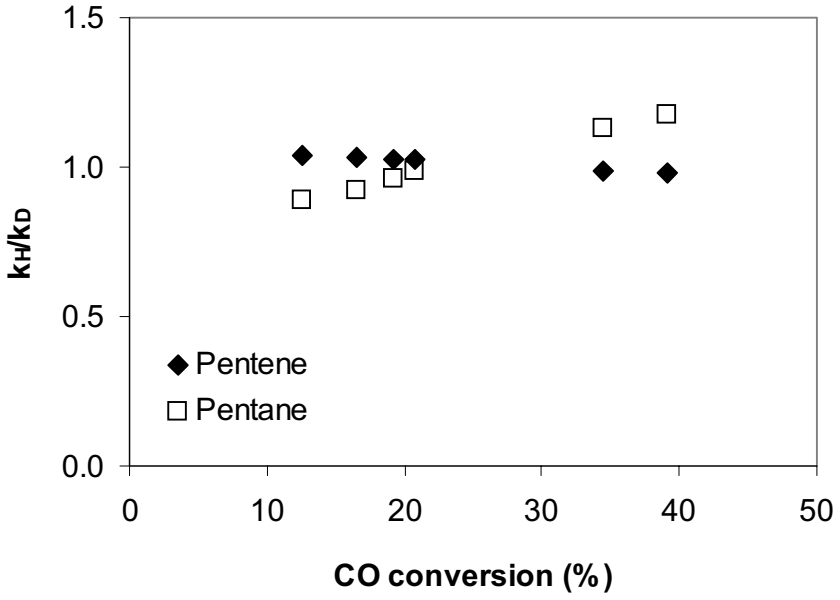

Figure 2.7. Isotope effect for C_5 products versus CO conversion (21.9 wt% Co/SiO_2, 200°C, 20 atm, H_2/CO or D_2/CO = 2.0)

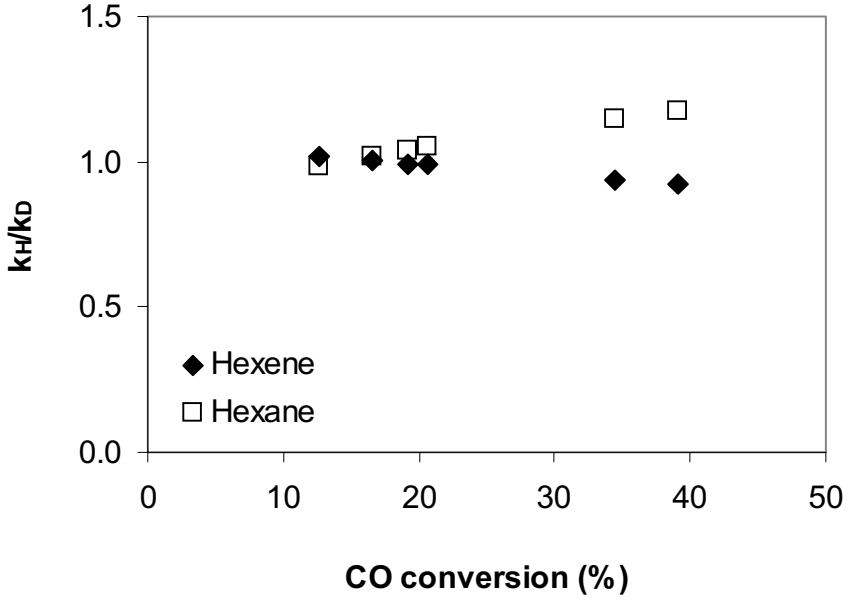

Figure 2.8. Isotope effect for C_6 products versus CO conversion (21.9 wt% Co/SiO_2, 200°C, 20 atm, H_2/CO or D_2/CO = 2.0)

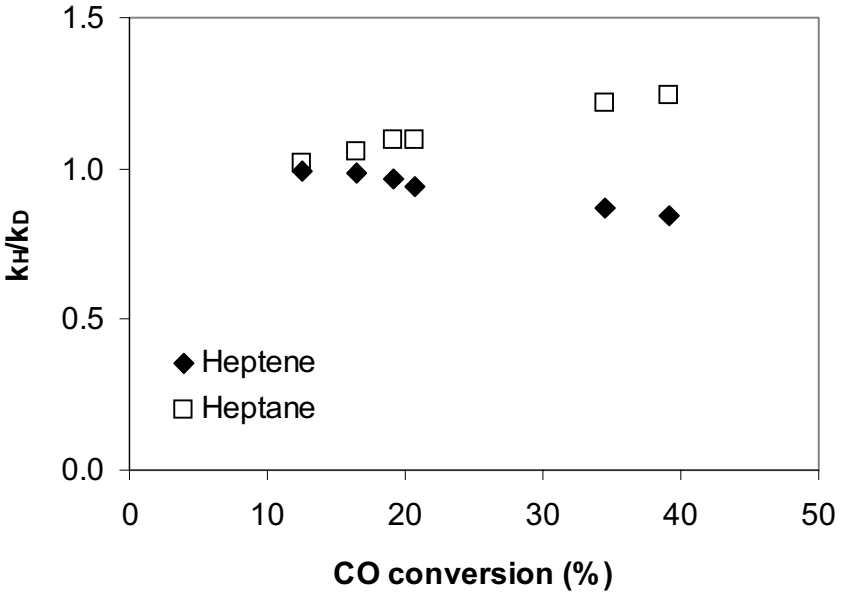

Figure 2.9. Isotope effect for C_7 products versus CO conversion (21.9 wt% Co/SiO_2, 200°C, 20 atm, H_2/CO or D_2/CO = 2.0)

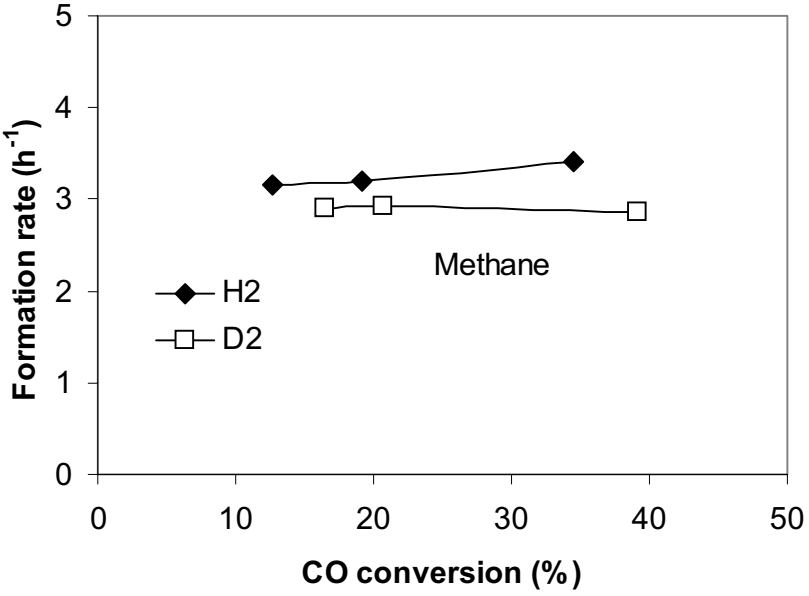

Figure 2.10. Rate of methane formation versus CO conversion (21.9 wt% Co/SiO_2, 200°C, 20 atm, H_2/CO or D_2/CO = 2.0)

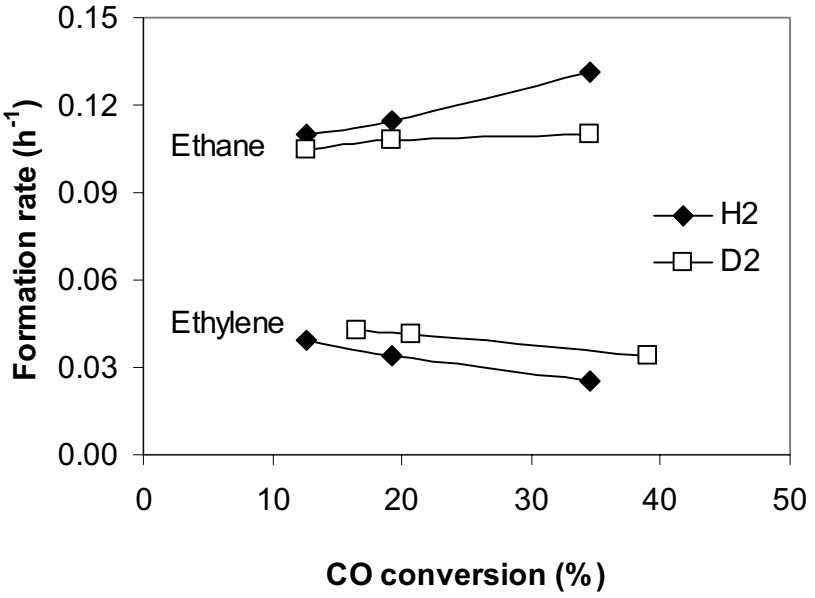

Figure 2.11. Rate of formation of C_2 products versus CO conversion (21.9 wt% Co/SiO_2, 200°C, 20 atm, H_2/CO or D_2/CO = 2.0)

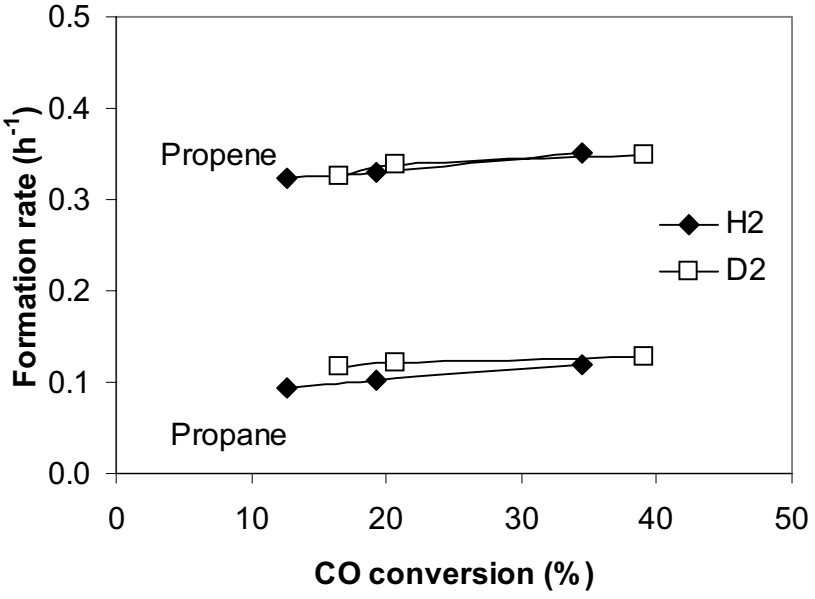

Figure 2.12. Rate of formation of C_3 products versus CO conversion (21.9 wt% Co/SiO_2, 200°C, 20 atm, H_2/CO or D_2/CO = 2.0)

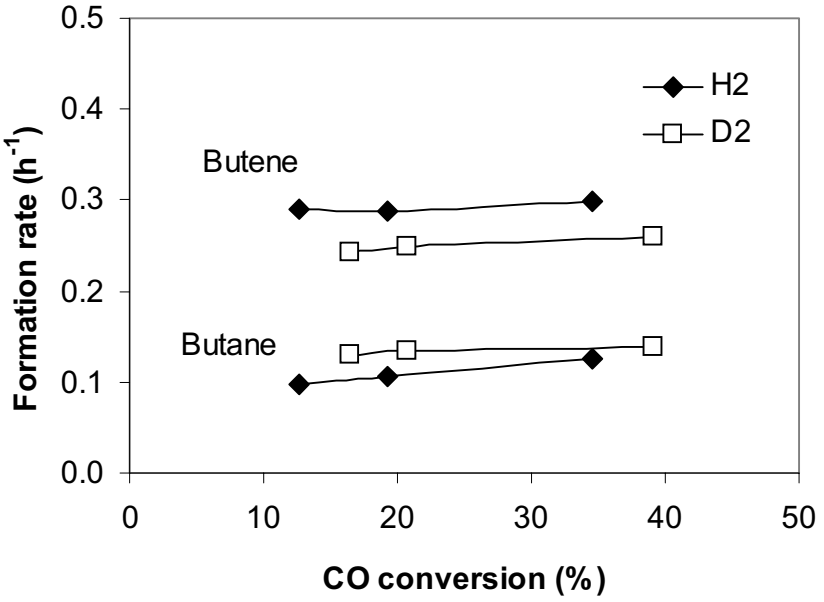

Figure 2.13. Rate of formation of C_4 products versus CO conversion (21.9 wt% Co/SiO_2, 200°C, 20 atm, H_2/CO or D_2/CO = 2.0)

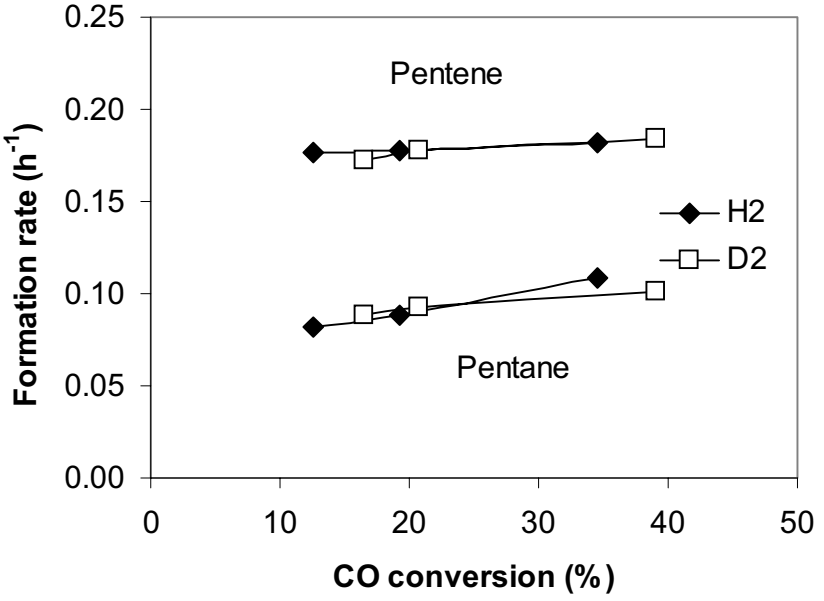

Figure 2.14. Rate of formation of C_5 products versus CO conversion (21.9 wt% Co/SiO_2, 200°C, 20 atm, H_2/CO or D_2/CO = 2.0)

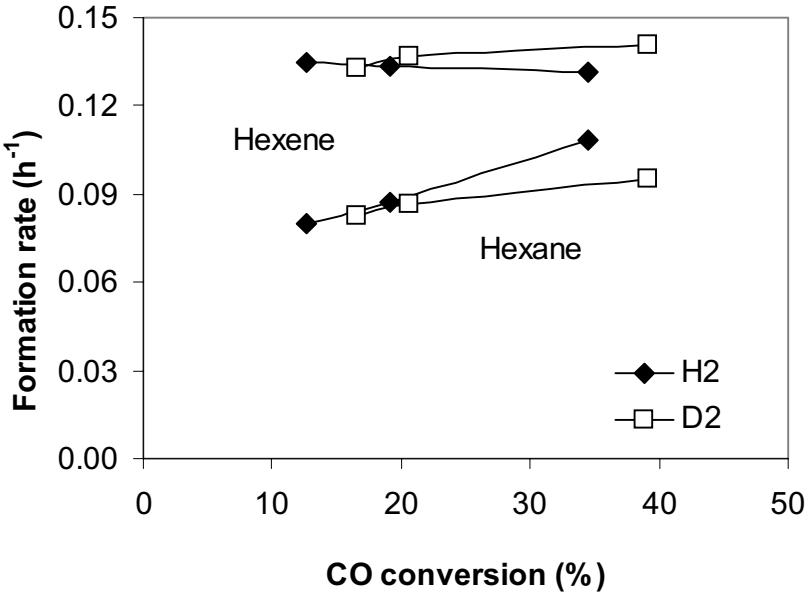

Figure 2.15. Rate of formation of C_6 products versus CO conversion (21.9 wt% Co/SiO_2, 200°C, 20 atm, H_2/CO or D_2/CO = 2.0)

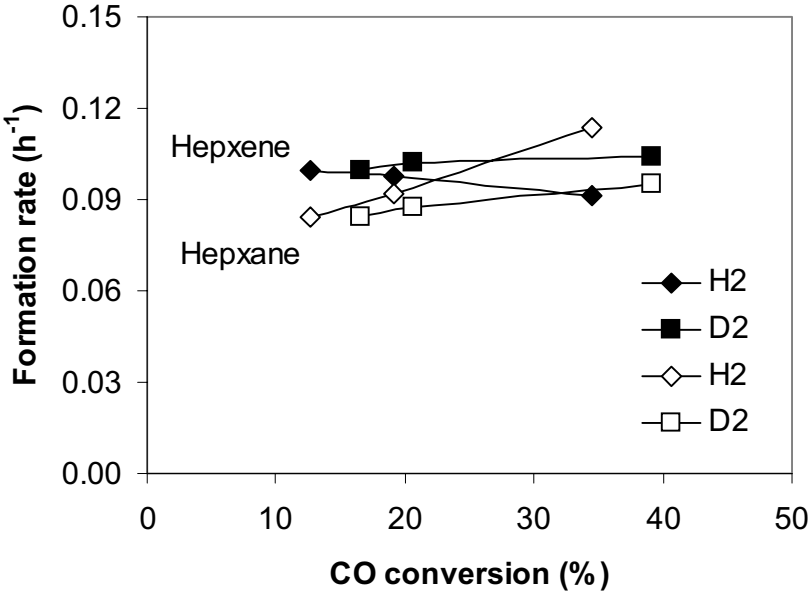

Figure 2.16. Rate of formation of C_7 products versus CO conversion (21.9 wt% Co/SiO_2, 200°C, 20 atm, H_2/CO or D_2/CO = 2.0)

The observed isotope effect for each hydrocarbon may result from a combination of kinetic and equilibrium isotopic effects which arise from individual elementary steps. Thus, the presence or absence of an overall isotope effect cannot be used to identify the rate-determining step [30,31]. But we may explain some of the results qualitatively. As mentioned above, the alkyl groups react to form olefins and paraffins via either hydrogen elimination or addition. The former process favors the reaction of D_2 because formation of a C-D bond is easier. Conversely, the latter process favors the reaction of H_2 because breaking of a C-H bond is easier. Therefore, the observed isotope effects (k_H/k_D) are generally inverse for paraffins whereas normal for olefins when we do not consider the effect of secondary reactions. The isotope effect (k_H/k_D = 0.8) for the overall CO consumption is very close to the effects for paraffins (k_H/k_D = 0.7-0.9, at zero conversion). This is reasonable because the dominant FTS products on Co are paraffins [4].

3.2 Proposed Mechanism

In last quarterly report, we proposed a water-enhanced monomer formation pathway in order to explain the enhancement of the synthesis rate by water observed on cobalt catalysts. In this mechanism, two parallel routes that determine the CO consumption rate were assumed, *i.e.*, adsorbed C* being hydrogenated to form CH* or reacting with adsorbed water to form CHOH* intermediates. A kinetic rate expression was then obtained according to this mechanism.

$$r_{-CO} = aP_{CO}^{1/2}P_{H2}^{1/4}(bP_{H2}^{1/2} + cP_{H2O})^{1/2}/(1 + dP_{H2}^{1/2} + eP_{H2O} + fP_{CO}^{1/2})^2 \qquad (1)$$

During this reporting period, another mechanism was taken into account for the positive water effect. Earlier studies suggest that the surface of Co is covered almost entirely by non-dissociated CO during FTS [26,27]. Hydrogen-assisted CO dissociation has also been considered as a rate-limiting step in FTS [32]. Here, we assumed that both H_2 and H_2O could promote the dissociation of adsorbed CO, which control the CO consumption rate. Then, we have the follow elementary steps.

1. $H_2 + 2* \leftrightarrow 2H*$
2. $CO + * \leftrightarrow CO*$
3. $CO* + H* \rightarrow C* + OH*$
4. $CO* + OH_2* \rightarrow C* + 2OH*$
5. $O* + H* \rightarrow OH* + *$
6. $OH* + H* \rightarrow OH_2* + *$
7. $OH_2* \leftrightarrow H_2O + *$

A rate expression was obtained according to the proposed mechanism,

$$r_{-CO} = (aP_{CO}P_{H2}^{1/2} + bP_{CO}P_{H2O})/(1 + cP_{H2}^{1/2} + dP_{H2O} + eP_{CO})^2, \qquad (2)$$

where,

$a = K_1^{1/2} K_2 k_3$
$b = K_2 k_4 (K_7)^{-1}$
$c = K_1^{1/2}$
$d = (K_7)^{-1}$
$e = K_2$

3.3 FTS Kinetic Study on Co-based Catalysts

Reaction kinetic studies were continued by running FTS with a 21.9 wt% Co/SiO_2 catalyst at 200 ^oC. This time we focused on the effect of water on synthesis rate by adding 0.5-2.0 atm water to the reacting feed (12 atm H_2 and 6 atm CO). CO conversion and selectivities of primary hydrocarbons (up to C_{12}) were measured at steady state. The experimental results are presented in Table 2.1. The overall CO consumption rate data along with those obtained from the previous kinetic run would be fitted to the above two rate expressions with multivariable non-linear regression. We were working on a macro program, which will optimize the regression (using Sigmaplot 5.0) and thus yield the best fit. This may let us distinguish which expression fits our experiment data better.

Table 2.1 Experimental results of FTS kinetic study over a 21.9 wt% Co/SiO_2 catalyst*

No	Partial Pressure (Catalyst Bed, atm)			Syngas Space Velocity	CO Conv	CO Conv Rate	CH_4 Formation Rate
	H_2	CO	H_2O	cc/min	(%)	(h^{-1})	(h^{-1})
1	11.4	5.3	0.6	32.8	20.8	58.3	5.2
2	12.0	5.9	0.2	64.2	5.5	31.2	4.3
3	10.9	2.6	0.3	52.0	19.1	53.6	7.1
4	10.6	2.4	0.4	40.2	28.3	59.0	7.3
5	10.7	1.3	0.2	92.1	22.5	63.1	12.0
6	11.5	8.6	0.3	50.3	6.2	35.2	3.5
7	12.0	5.9	0.2	64.2	5.9	33.5	4.3
8	12.0	5.9	0.8	64.2	9.3	52.8	4.5
9	11.7	5.7	1.3	64.2	11.0	62.5	4.4
10	11.6	5.7	2.4	64.2	12.5	71.0	4.4
11	12.2	5.7	0.2	57.7	6.0	29.8	3.7

* Reaction conditions: 200°C, H_2/CO ratio from 1.3 to 8.5, water partial pressure up to 2 atm, reaction pressure from 13 to 22 atm,

III. REFERENCES

1. M. E. Dry, The Fisher-Tropsch Synthesis, in *Catalysis-Science and Technology*, Vol. 1, p. 160, J. R. Anderson and M. Boudart eds., Springer Verlag, New York, 1981.
2. F. Fischer and H. Tropsch, *Brennstoff-Chem.* **7** (1926) 97.
3. R. B. Anderson, in *Catalysis* Vol. 4, p. 29, P. H. Emmett eds., Van Nostrand-Reinhold, New York, 1956.
4. H. H. Storch, N. Golumbic and R. B. Anderson, *The Fischer-Tropsch and Related Syntheses*, Wiley, New York, 1951; R. B. Anderson, *The Fischer-Tropsch Synthesis*, Wiley, New York, 1984.
5. H. Kolbel and M. Ralek, *Catal. Rev.-Sci. Eng.* **21** (1980) 225.
6. J. W. Niemantsverdriet and A. M. van der Kraan, *J. Catal.* **72** (1981) 385.
7. J. A. Amelse, J. B. Butt and L. J. Schwartz, *J. Phys. Chem.* **82** (1978) 558.
8. G. B. Raupp and W. N. Delgass, *J. Catal.* **58** (1979) 348.
9. R. Dictor and A. T. Bell, *J. Catal.* **97** (1986) 121.
10. J. P. Reymond, P. Meriaudeau and S. J. Teichner, *J. Catal.* **75** (1982) 39.
11. C. S. Kuivila, P. C. Stair and J. B. Butt, *J. Catal.* **118** (1989) 299.
12. C. S. Huang, L. Xu and B. H. Davis, *Fuel Sci. Tech. Int.* **11** (1993) 639.
13. E. Iglesia, and S. C. Reyes, R. J. Madon and S. L. Soled, *Advances in Catalysis*, Vol. 39, p. 221, Academic Press, 1993.
14. E. Iglesia, *Appl. Catal. A: General* **161** (1997) 59.
15. S. Soled, E. Iglesia and R. A. Fiato, *Catal. Lett.* **7** (1990) 271.
16. S. Soled, E. Iglesia, S. Miseo, B. A. DeRites and R. A. Fiato, *Topics in Catal.* **2** (1995) 193.
17. E. Iglesia, A research proposal submitted to the Division of Fossil Energy.
18. M. T. Xu, E. Iglesia, *J. Phys. Chem. B* **102(6)**, 961-966, 1998.
19. A. P. Raje, R. J. O'Brien and B. H. Davis, *J. Catal.* **180** (1998) 36.
20. A. F. Wells, *Structural Inorganic Chemistry*, Oxford, 1945.
21. T. P. Wilson, *J. Catal.* **60**, 167 (1979).
22. T. Soller, S. Goldwasser and R.A. Beebe, *J. Am. Chem. Soc.,* **58**, 1703 (1936).
23. F. de Pauw, J. C. Jungers, *Bull. Soc. Chim. Belg*., **57**, 618 (1948).
24. J. Nicolai, M. Hont and J.C. Jungers, *Bull. Soc. Chim. Belg*., **55**, 160 (1946).
25. G. A Huff, and C. N. Satterfild, *Ind. Eng. Chem. Res.* **23**, 696 (1984).
26. H. H. Storch, N. Golumbic and R. B. Anderson, *The Fischer-Tropsch and Related Syntheses*, Wiley, New York, 1951; R. B. Anderson, *The Fischer-Tropsch Synthesis*, Wiley, New York, 1984.
27. A. T. Bell, *Catal. Rev. Sci. Eng*. **23 (1&2)** (1981) 203.
28. M. M., Sakharov and E. S., Dokukina, *Kinet. Katal*. **2** (1961) 710.
29. D. W., Mckee, *J. Catal.* **8** (1967) 240.
30. T. P., Wilson, *J. Catal.* **60** (1979) 167.
31. C. S., Kellner and A. T. Bell, *J. Catal.* **67** (1981) 175.
32. H. H. Nijs, and P. A. Jacobs, *J. Catal.* **66** (1980) 401.

Task 12. Reporting/Project Management

One quarterly and three monthly reports have been completed.